Bone 150 (2021) 116010

Contents lists available at ScienceDirect

Bone

journal homepage: www.elsevier.com/locate/bone

Full Length Article

Odontoblast death drives cell-rich zone-derived dental tissue regeneration

Lijuan Zhao [a], Shinichirou Ito [b], Atsushi Arai [c], Nobuyuki Udagawa [d], Kanji Horibe [e], Miroku Hara [f], Daisuke Nishida [g], Akihiro Hosoya [h], Rinya Masuko [i], Koji Okabe [j], Masashi Shin [j,k], Xianqi Li [l], Koichi Matsuo [m], Shinichi Abe [n], Satoru Matsunaga [n], Yasuhiro Kobayashi [a], Hideaki Kagami [a], Toshihide Mizoguchi [a,g,*]

[a] Institute for Oral Science, Matsumoto Dental University, Nagano, Japan
[b] Department of Oral and Maxillofacial Surgery, Tokyo Dental College, Tokyo, Japan
[c] Department of Orthodontics, Matsumoto Dental University, Nagano, Japan
[d] Department of Oral Biochemistry, Matsumoto Dental University, Nagano, Japan
[e] Department of Oral Histology, Matsumoto Dental University, Nagano, Japan
[f] Department of Oral Diagnostics and Comprehensive Dentistry, Matsumoto Dental University Hospital, Nagano, Japan
[g] Oral Health Science Center, Tokyo Dental College, Tokyo, Japan
[h] Division of Histology, School of Dentistry, Health Science University of Hokkaido, Hokkaido, Japan
[i] JEOL Ltd., Tokyo, Japan
[j] Section of Cellular Physiology, Department of Physiological Sciences and Molecular Biology, Fukuoka Dental College, Fukuoka, Japan
[k] Oral Medicine Center, Fukuoka Dental College, Fukuoka, Japan
[l] Department of Oral and Maxillofacial Surgery, Matsumoto Dental University, Nagano, Japan
[m] Laboratory of Cell and Tissue Biology, Keio University School of Medicine, Tokyo, Japan
[n] Department of Anatomy, Tokyo Dental College, Tokyo, Japan

ARTICLE INFO

Keywords:
Cell-rich zone
Dental tissue regeneration
Odontoblast
Odontoblast-like cell
Nestin
PTH1R

ABSTRACT

Severe dental tissue damage induces odontoblast death, after which dental pulp stem and progenitor cells (DPSCs) differentiate into odontoblast-like cells, contributing to reparative dentin. However, the damage-induced mechanism that triggers this regeneration process is still not clear. We aimed to understand the effect of odontoblast death without hard tissue damage on dental regeneration. Herein, using a Cre/LoxP-based strategy, we demonstrated that cell-rich zone (CZ)-localizing Nestin-GFP-positive and Nestin-GFP-negative cells proliferate and differentiate into odontoblast-like cells in response to odontoblast depletion. The regenerated odontoblast-like cells played a role in reparative dentin formation. RNA-sequencing analysis revealed that the expression of odontoblast differentiation- and activation-related genes was upregulated in the pulp in response to odontoblast depletion even without damage to dental tissue. In this regenerative process, the expression of type I parathyroid hormone receptor (PTH1R) increased in the odontoblast-depleted pulp, thereby boosting dentin formation. The levels of PTH1R and its downstream mediator, *i.e.*, phosphorylated cyclic AMP response element-binding protein (Ser133) increased in the physically damaged pulp. Collectively, odontoblast death triggered the PTH1R cascade, which may represent a therapeutic target for inducing CZ-mediated dental regeneration.

Abbreviations: PTHrP, type I PTH/PTH-related peptide; PTH1R, type I parathyroid hormone receptor; CZ, cell-rich zone; DPSCs, dental pulp stem and progenitor cells; BM-MSPCs, bone marrow mesenchymal stem and progenitor cells; αSMA, alpha-smooth muscle actin; GFP, green fluorescent protein; Nes, nestin; Col1, type I collagen α; PFA, paraformaldehyde; BSA, bovine serum albumin; SD, standard deviation; DT, diphtheria toxin; DTR, DT receptor; Dspp, dentin sialophosphoprotein; EdU, 5-ethynyl-2′-deoxyuridine; μ-CT, microcomputed tomography; Ab, alveolar bone; GSEA, gene set enrichment analysis; RNA-seq, RNA-sequencing; TPM, transcript kilobase per million; GO, gene ontology; Bglap, bone gamma-carboxyglutamate protein; Runx2, runt-related transcription factor 2; PDL, periodontal ligament; CREB, cyclic AMP response element-binding protein; MAR, mineral apposition rate; Osmr, oncostatin M receptor; Il27ra, IL-27 receptor alpha; MTA, mineral trioxide aggregate; MFM, maxillary first molar.

* Corresponding author at: Oral Health Science Center, Tokyo Dental College, Tokyo 101-0061, Japan.
E-mail address: tmizoguchi@tdc.ac.jp (T. Mizoguchi).

https://doi.org/10.1016/j.bone.2021.116010
Received 15 April 2021; Received in revised form 10 May 2021; Accepted 12 May 2021
Available online 18 May 2021

1. Introduction

The bone tissue is constantly resorbed by osteoclasts and replaced with the newly formed bone tissue by osteoblasts [1,2]. Although the average lifetime of mature osteoblasts is limited, their counts are continuously maintained by bone marrow mesenchymal stem and progenitor cells (BM-MSPCs), which exhibit the potential for self-renewal and differentiation into mesenchymal lineages in the bone marrow [3–6]. Studies indicate that dental pulp tissue also contains a multipotent stromal population, known as dental pulp stem and progenitor cells (DPSCs) [7–9]. Although controversial, several reports suggest that the DPSC population is identified as neural-glial antigen 2^+ pericytes [10], glioma-associated oncogene 1^+ cells [11], or proteolipid protein 1^+ glial cells [12] in the incisors and alpha-smooth muscle actin $(\alpha SMA)^+$ perivascular cells [13] or $Axin2^+$ cells [14] in the molars. In contrast to osteoblasts, dentin-forming odontoblasts reside within the dental tissue for a long term; therefore, DPSCs do not differentiate into odontoblasts in healthy fully formed teeth [15]. However, when odontoblast death occurs as a result of severe tooth damage, the DPSCs proliferate and differentiate into odontoblast-like cells that contribute to reparative dentin formation [10,11,14,16,17]. However, how odontoblast death is associated with the mechanisms underlying reparative dentin formation remains unclear.

The cell-rich zones (CZs) adjacent to the odontoblast layer in the dental pulp have been reported to contain odontoblast progenitor cells [18–20], which can be specifically detected in Nestin (*Nes*) reporter mice, wherein the gene encoding green fluorescent protein (*GFP*) is driven by the enhancer element of the second intron of *Nes* and minimal promoter of the heat shock protein-68 gene [21,22]. Furthermore, BM-MSPCs can be labeled based on Nes-GFP expression in another *Nes-GFP* line, which expresses *GFP* under the control of the 5.8-kb promoter and 1.8-kb fragment of the second intron of *Nes* [23–25]. Although these reports suggest that the *Nes-GFP* lines are useful for detecting the precursor population of hard tissue-forming cells, whether the Nes-GFP-positive population contributes to dental tissue regeneration and neoformation of odontoblast-like cells in the dental pulp remains elusive.

The biologically active N-terminal 1–34 peptide of the human parathyroid hormone [PTH (1–34)] exerts a bone anabolic activity and is therefore used clinically for the treatment of patients with osteoporosis. Previous studies have suggested that one of the mechanisms underlying the therapeutic action of PTH (1–34) is the positive regulation of BM-MSPC osteoblastogenesis [26–28]. The type I PTH/PTH-related peptide (PTHrP) receptor (PTH1R) has been reported to be expressed by diverse dental mesenchymal cell types, including odontoblasts, dental pulp cells, and dental follicle cells, during the neonatal period and contributes to root formation [29,30]. These reports suggest that the activation of additional signaling pathways downstream of PTH1R may positively affect the recovery of damaged dental tissue; however, experimental validation is still required.

Therefore, to understand the mechanistic details of dental tissue regenerative processes, herein, we induced Cre/LoxP-mediated odontoblast-specific cell death and found that this process significantly affects the dental pulp environment in triggering tissue regeneration.

2. Materials and methods

2.1. Experimental animals

C57BL/6 mice were purchased from Japan SLC (Shizuoka, Japan). *B6.FVB-Tg(Col1a1-cre)1Kry* mice (*Col1(2.3)-Cre*) (RBRC0503) [31] were purchased from RIKEN BRC (Ibaraki, Japan). *C57BL/6-Gt(ROSA)26Sor$^{tm1(HBEGF)Awai}$/J* (*iDTR*) (JAX007900) mice were purchased from Jackson Laboratory (Bar Harbor, ME, USA). *Col1(2.3)-GFP* [32] mice were generated in one of the authors' laboratories (K.M.). *Nes-GFP* [23,25] mice were kindly provided by G. Enikolopov from Stony Brook University. All mice used for the experiments belonged to the C57BL/6 strain, and their weight and age ranges were 5–28 g and 7 days to 24 weeks, respectively. During the experiments, euthanasia was performed by cervical spine fracture dislocation under anesthesia with isoflurane (Pfizer Inc., New York City, NY). Mice were fed with a regular diet (MF; Oriental Yeast Co., Ltd., Tokyo, Japan). Mice >12 weeks of age were used for DT-induced odontoblast depletion experiments because dentinogenesis (depending on development) was rarely observed at 12 weeks of age (Fig. 4A). To reduce the number of mice euthanized, both male and female mice were used in this study. The maximal number of mice per cage was five. All mice were housed under specific pathogen-free conditions at 24 ± 2 °C, exposed to 50–60% humidity with a 12-h light/dark cycle, and provided with sterile water and *ad libitum* access to food in animal facilities certified by the Animal Care and Use Committees of Tokyo Dental College (Tokyo, Japan) or Matsumoto Dental University (Nagano, Japan). Animal studies were approved—and performed in accordance with the guidelines provided—by the ARRIVE and Animal Care Committee of Tokyo Dental College (Tokyo, Japan) and Matsumoto Dental University (Nagano, Japan).

2.2. Antibodies and reagents

The list of antibodies and reagents used for immunostaining is shown in Table S1. PTH (1–34) was provided by Asahi Kasei Pharma Corporation (Tokyo, Japan). Dissection, sectioning, and staining for each experiment were always performed at the same time and conditions.

2.3. Microscopy and histomorphometry

Mice were perfused with 4% paraformaldehyde (PFA) for fixation. The maxillae were removed and further fixed with 4% PFA for 24 h at 4 °C.

To perform imaging analysis of the paraffin-embedded tissue, the maxilla was dissected and decalcified in 10% EDTA for 3 weeks at 4 °C. Paraffin-embedded 4-μm-thick sections were used for hematoxylin and eosin staining or immunohistochemistry. The sections were incubated with primary antibodies overnight at 4 °C, and immunoreactivity was visualized using Histofine Simple Stain Mouse MAX PO (R) (Nichirei Biosciences Inc., Tokyo, Japan) and ImmPACT DAB Substrate (Vector Laboratories, Burlingame, CA) according to the manufacturers' instructions; the samples were counterstained with hematoxylin. Bright-field images were acquired using an Axioskop2 plus equipped Plan-NEOFLUAR (2.5×/0.075, 10×/0.30, 20×/0.50, 40×/0.75) and AxioVision Rel. 4.8 (all from Carl Zeiss, Oberkochen, Germany).

To perform imaging analysis of the cryosections, the dissected maxilla was decalcified using 20% Morse solution (Fujifilm Wako Pure Chemical, Osaka, Japan) for 24 h at 4 °C (or used without decalcification) and subsequently incubated with 10%, 20%, and 30% sucrose solutions for more than 2 h at 4 °C for cryoprotection. The samples were then embedded in super cryo-embedding medium (Section-Lab, Hiroshima, Japan). Cryosections, 10-μm-thick, were cut in accordance with Kawamoto's film method [33] using Cryofilm type IIIC and a tungsten carbide knife (Section-Lab). The sections were incubated with primary antibodies overnight at 24 ± 2 °C, however, in case of staining with rabbit anti-pCREB (Ser133) antibody coupled to AF 488 (87G3) or rat anti-CD31 antibody coupled to PE (MEC13.3), the tissue was pretreated with 0.25% Triton X-100 for 15 min at 24 ± 2 °C. The sections were further incubated with secondary antibodies for 2 h at 24 ± 2 °C, mounted using 30% glycerol, covered with coverslips, and sealed with nail polish. Z stacks of confocal images were obtained at 1-μm intervals between 10-μm-thick sections. Fluorescence images were acquired using a laser-scanning confocal microscope (Axio Observer, LSM510 and LSM880) equipped with Plan-APOCHROMAT (20×/0.8) and ZEN 2.3 black edition (Carl Zeiss). $Col1(2.3)^+$ cells in the dental pulp of molars were calculated based on the frequency of $Col1(2.3)^+$ cell surfaces per dentin surface localized above the pulp floor (Fig. 1F). The area corresponding to a single pulp horn of a molar (1.3×10^4–2.0×10^5 μm^2),

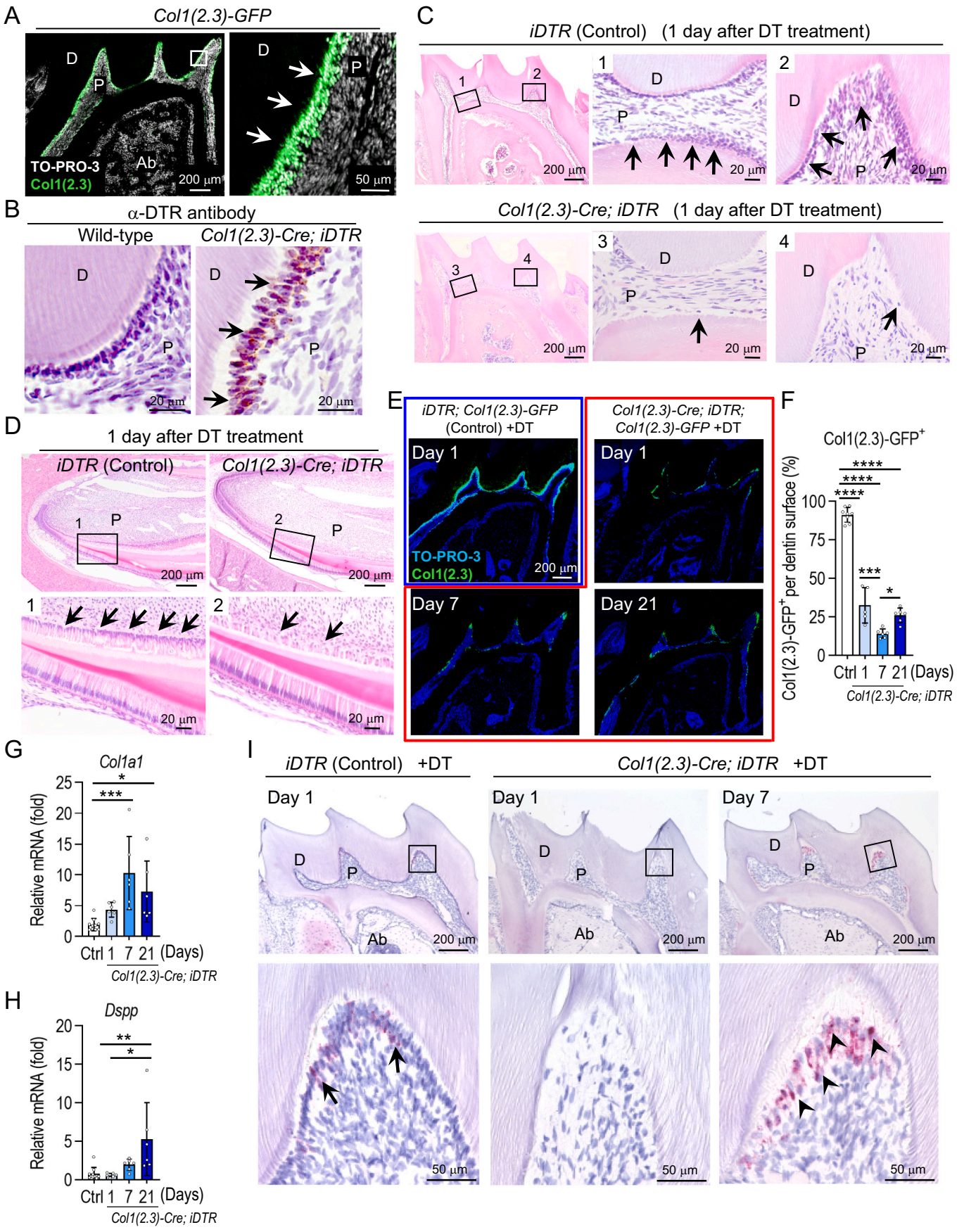

(caption on next page)

Fig. 1. The depleted odontoblast population is readily replenished.
A. Confocal images (Z stack) showing odontoblast-specific Col1(2.3)-GFP expression in thick maxillary first molar (MFM) sections of 12-week-old *Col1(2.3)-GFP* mice. Arrows: Col1(2.3)-GFP$^+$ odontoblasts. Scale bar = 200 μm. Right panel shows the magnified view of the boxed area. Scale bar = 50 μm. n = 3. **B.** Images showing odontoblast-specific diphtheria toxin receptor (DTR) expression in MFM sections of 12-week-old *Col1(2.3)-Cre; iDTR* mice. Arrows: DTR$^+$ odontoblasts. Scale bar = 20 μm. n = 3. **C–I.** Twelve-week-old *Col1(2.3)-Cre; iDTR* and *iDTR* (control) mice (C, D, and G–I) or *Col1(2.3)-Cre; iDTR; Col1(2.3)-GFP* and *iDTR; Col1(2.3)-GFP* (control) mice (E and F) were treated with diphtheria toxin (DT) (250 ng/day) for 1 week and analyzed at the indicated time points after the final DT injection. (C and D) Hematoxylin and eosin (HE) staining showed depleted odontoblasts in MFMs (C) and maxillary incisors (D). Arrows: odontoblasts. Scale bar = 200 μm. Numbered panels represent magnified views of the boxed areas. Scale bar = 20 μm. C: Control: n = 3, *Col1(2.3)-Cre; iDTR*: n = 3, D: Control: n = 3, *Col1(2.3)-Cre; iDTR*: n = 3. (E and F) Confocal images (Z stack) (E) and quantification [F: percentage of Col1(2.3)-GFP$^+$ surfaces per dentin surface above the pulp floor] of Col1(2.3)-GFP$^+$ cells in thick MFM sections. Scale bar = 200 μm. Control: n = 7 (8 MFMs), *Col1(2.3)-Cre; iDTR* (day 1): n = 3 (5 MFMs), (day 7): n = 5 (6 MFMs), (day 21): n = 3 (6 MFMs). One-way analysis of variance (ANOVA) followed by Tukey's test. (G and H) Real-time PCR for *Col1a1* and *Dspp*, Control: n = 10 (10 MFMs), *Col1(2.3)-Cre; iDTR* (day 1): n = 3 (6 MFMs), (day 7): n = 4 (6 MFMs), (day 21): n = 3 (6 MFMs). One-way ANOVA followed by Kruskal-Wallis test. (I) *in situ* hybridization for *Dspp*. Arrows: *Dspp*$^+$ odontoblasts, arrowheads: *Dspp*$^+$ odontoblast-like cells. Scale bar = 200 μm. Lower panels show the magnified view of the boxed area. Scale bar = 50 μm. Control: n = 3, *Col1(2.3)-Cre; iDTR* (day 1): n = 3, (day 7): n = 3. Nuclei were visualized using TO-PRO-3. P: pulp, D: dentin, Ab: alveolar bone, Ctrl: control. *$p < 0.05$, **$p < 0.01$, ***$p < 0.001$, ****$p < 0.0001$. Data are represented as mean ± standard deviation (SD).

including the tip area, was quantified in every other image.

2.4. iDTR-mediated cell depletion

For DT-mediated cell depletion, 250 ng of DT (Sigma-Aldrich, St. Louis, MO) was injected intraperitoneally every 24 h for 1 week; subsequently, mice were analyzed for 1–70 days after final DT treatment.

2.5. Calcein and PTH (1–34) treatments

Mice were injected with 160 μL calcein (Sigma-Aldrich) (3 mg/mL) subcutaneously according to each experimental time-course. Details of the experimental time courses are shown in Fig. S1. As shown in Fig. 4A, 4–12-week-old wild-type mice were injected twice at an interval of 4 days and analyzed 1 day after the final calcein injection (Fig. S1A). Calcein was injected 3 and 6 days after the final DT injection, and the dentin tissue was used for imaging analysis on day 7 (Figs. 4B, S1B). One day after the final DT injection, mice were intraperitoneally injected with 80 μg/kg human PTH (1–34) (Asahi Kasei Pharma Corporation) every 12 h for 16 days, with calcein injection (twice) on days 11 and 16 after the final DT injection and analyzed 1 day after the final calcein injection (Figs. 8, B and C, S1C). PTH (1–34) (80 μg/kg/12 h) (Asahi Kasei Pharma Corporation) was administered for 12 days after cavity preparation, and calcein was administered on days 2 and 12 during the course of PTH treatment; mice were analyzed 1 day after the final calcein injection (Figs. 9, C and D, S1D). Mice were perfused with 4% PFA, and the maxillary first molars were further fixed with 4% PFA for 24 h at 4 °C and subsequently incubated with 10%, 20%, and 30% sucrose solutions for more than 2 h at 4 °C for cryoprotection. Cryosections (10-μm-thick) were prepared using Kawamoto's film method, and images were captured using a laser-scanning confocal microscope as described in "Microscopy and histomorphometry." Seven points in the calcein double-labeled region were measured in the area of a single pulp horn (1.2×10^5 μm^2), and their average was used for calculating the MAR, *i.e.*, the distance between adjacent labeling lines per interval of labeling days. Mice were randomly assigned to the vehicle (0.1% bovine serum albumin [BSA]) or PTH (1–34) treatment group.

2.6. EdU incorporation experiments

One day after the final DT injection, the mice were intraperitoneally injected with 0.4 mg EdU (Thermo Fisher Scientific, Waltham, MA) every 24 h for 13 days and euthanized 1 day after the final EdU injection. EdU-positive cells were detected using the Click-iT Plus EdU Alexa Fluor™ 647 Imaging Kit (Thermo Fisher Scientific) as per the manufacturer's recommendations.

2.7. In situ hybridization

Four-micrometer-thick paraffin sections were prepared as described in "Microscopy and histomorphometry." *In situ* hybridization was performed using the RNAscope 2.5HD Reagent Kit-RED with probes for *Dspp* and *Pth1r* (Advanced Cell Diagnostics, Newark, CA).

2.8. RNA isolation

Extracted maxillary first molars were incubated with Hanks' balanced salt solution (HBSS) containing 0.1% collagenase IV, 0.2% dispase (Thermo Fisher Scientific), and 20 U/mL DNase (Worthington Biochemical, Lakewood, NJ) for 15 min at 37 °C to remove the PDL. Molars were washed with phosphate-buffered saline and homogenized in TRIzol (Thermo Fisher Scientific) using Tissue Lyser (Qiagen, Hilden, Germany), and total RNA was purified using a PureLink RNA Micro kit (Thermo Fisher Scientific).

2.9. Dental cavity preparation

A pulp-exposed cavity with a diameter of 0.5 mm was prepared in the maxillary first molars of 6–15-week-old mice, under anesthesia with pentobarbital sodium (30 mg/kg), using a steel bar (round, HP1/4, 005; Dentsply Sirona, Charlotte, NC) and micro motor handpiece (INTRAmatic 10C; KAVO Dental Excellence, Tokyo, Japan). The exposed cavity was capped with mineral trioxide aggregate (MTA) (TheraCal LC; Bisco, Schaumburg, IL) and closed with glass ionomer cement (FujiVII, GC, Tokyo, Japan). To prevent cement from detaching, opposing mandibular first molars were extracted, and 2 or 4 weeks later, the maxillary first molars were collected and used for imaging analysis.

2.10. Quantitative real-time PCR

Quantitative real-time PCR using purified total RNA was performed by One-Step SYBR Prime Script PLUS RT-PCR (Takara, Shiga, Japan). The PCR conditions were 42 °C for 5 min and 95 °C for 10 s for reverse transcription, followed by 40 cycles of 95 °C for 5 s and 60 °C for 30 s. Gene expression data were normalized to that of elongation factor-1 alpha gene, and relative expression was calculated using the standard curve method. Melting curve analyses of products were performed to ensure reaction specificity. The primers for each gene are shown in Table S2.

2.11. RNA-seq analysis

Reads were aligned to the reference mouse genome (Gencode GRCm38.p6.genome) using STAR (version 2.7) [34], and read counting was performed using RSEM (version 1.3.1) [35]. We restricted the analysis to genes with transcript kilobase per million (TPM) >1 in at least one sample. Raw reads of those genes were then normalized using the trimmed mean of M-values method in edgeR (version 3.26.8, R package). Differential expression analysis was performed using Fisher's exact test implemented in edgeR [36]. The adjusted *p*-value was

obtained using the Benjamini–Hochberg method [37]. Hierarchical clustering analysis was performed using Euclidean distance and the furthest neighbor method. We performed gene ontology (GO) analysis for the differentially expressed genes with adjusted p-value < 0.05 and absolute $\log_2$ fold change ≥ 0.5 using Metascape [38]. GSEA [39] was performed using GSEA software (v 4.0.3) with GO gene sets (c5.All.v7.0.symbols.gmt). Data analysis was performed by Genble Inc. (Fukuoka, Japan).

2.12. Microcomputed tomography

Mouse maxillary first molars were fixed in 70% ethanol for 1 week at 4 °C. Three-dimensional reconstructions of molars were generated using the Scanco Medical μ-CT 35 system. Hard tissue and pulp volume of the molars were analyzed using IPL Evaluation software (Scanco Medical, Bruttisellen, Switzerland). Microcomputed tomography (μ-CT) analysis was performed by an investigator blinded to the genotypes of the animals under investigation.

2.13. Statistical analyses

Statistical analyses were performed using GraphPad Prism 8.0 (GraphPad Software Inc., La Jolla, CA). The data were first analyzed using the Shapiro-Wilk test to evaluate whether they followed normal distribution. To compare two groups, equality of the two variances was assessed using the F-test. When the data sets met the test requirements for distribution as well as variance, Student's *t*-test was used to assess the significance. When the data did not follow normal distribution, a nonparametric Mann-Whitney *U* test was used. When the data variances were significantly different in the F-test, the Welch's *t*-test was used.

To compare multiple groups for significance, one-way ANOVA with Tukey's multiple comparison test was used when the data sets met the test requirements for distribution as well as variance. When the data did not follow normal distribution, a nonparametric Kruskal-Wallis test was used. All data investigated using one-way ANOVA with Tukey's multiple comparison test showed no significant difference in variances as assessed *via* the Brown-Forsythe test. The results were expressed as mean ± standard deviation (SD). $p < 0.05$ was considered significant.

3. Results

3.1. Odontoblasts are regenerated after depletion

To induce cell death specifically in the odontoblasts using a Cre/LoxP-based strategy, we confirmed the odontoblast-specific expression pattern of GFP in type I collagen α [*Col1(2.3)*]-*GFP* mice, in which GFP is expressed under the control of a 2.3-kb fragment of the *Col1* promoter [29,32,40]. Consistent with previous reports, GFP expression was only observed in odontoblasts in the maxillary first molars of *Col1(2.3)-GFP* mice (Fig. 1A, arrows: Col1(2.3)-GFP$^+$ odontoblasts). Based on these observations, we bred *Col1(2.3)-Cre* and inducible diphtheria toxin (DT) receptor (DTR; *ROSA26-loxP-stop-loxP-DTR: iDTR*) mice. In this mouse model, Cre recombinase is expressed in the Col1(2.3)$^+$ odontoblasts and subsequently removes the DTR stop codon leading to its expression; therefore, odontoblasts are specifically depleted by DT treatment. We confirmed the odontoblast-specific expression of DTR in dental tissue using an anti-DTR antibody (Fig. 1B, arrows: DTR$^+$ odontoblasts). The *Col1(2.3)-Cre; iDTR* mice were injected with DT for 1 week (250 ng/day), and it was confirmed that odontoblasts had dramatically depleted in both maxillary first molars and incisors 1 day after the final DT injection (Fig. 1C and D, arrows: odontoblasts). To determine whether odontoblast counts recover post depletion, we generated *Col1(2.3)-Cre; iDTR; Col1(2.3)-GFP* mice, in which odontoblasts can be monitored as GFP-positive cells. The odontoblast population significantly decreased 1 day after odontoblast depletion in *Col1(2.3)-Cre; iDTR; Col1(2.3)-GFP* mice compared with that in control mice (Fig. 1E; quantification of Col1(2.3)-GFP$^+$ cell surfaces per dentin surface (%) is shown in Fig. 1F). The Col1(2.3)-GFP$^+$ cell counts further decreased until 7 days after final DT treatment; however, they recovered significantly on day 21 (Fig. 1, E and F). Furthermore, real-time PCR showed that *Col1a1* mRNA expression in the molars 7 days after odontoblast depletion was higher than that after 1 day, suggesting that the recovery of odontoblasts was initiated before day 7 (Fig. 1G). Consistent with these data, the mRNA levels of dentin sialophosphoprotein (*Dspp*)—an essential marker of odontoblast differentiation—decreased 1 day after odontoblast depletion but recovered by day 7 (Fig. 1, H and I, arrows: *Dspp*$^+$ odontoblasts, arrowhead: recovered *Dspp*$^+$ odontoblast-like cells). The odontoblast regeneration reached a plateau 21 days after the final DT treatment (Fig. S2). Altogether, these findings suggest that the dental pulp environment is modified upon odontoblast depletion, which promptly triggers the odontoblastogenesis of immature cells.

3.2. Odontoblast depletion induces odontoblast precursors to proliferate and differentiate into odontoblast-like cells

Considering that the cell cycle progression of pulp cells is essential for dental tissue damage-induced odontoblastogenesis, we next analyzed the cell cycle status of the dental pulp cells in odontoblast-depleted molars [10,11,14,16,17]. Ki67-positive proliferating cells were more abundant in *Col1(2.3); iDTR* tissues 1 day after odontoblast depletion than in control tissues (Fig. 2A, arrows: Ki67$^+$ cells; quantification is shown in Fig. 2B). Real-time PCR indicated that the *Ki67* mRNA significantly increased in the molars 1 day after odontoblast depletion, albeit transiently, suggesting that the proliferation of dental pulp cells was triggered by odontoblast death (Fig. 2C).

Furthermore, we analyzed whether these proliferating pulp cells differentiate into odontoblast-like cells, by performing lineage tracing analysis of 5-ethynyl-2′-deoxyuridine (EdU)-labeled cells. EdU was administered daily for 13 days; EdU administration was initiated 1 day after odontoblast depletion in *Col1(2.3)-Cre; iDTR; Col1(2.3)-GFP* mice. Col1(2.3)-GFP$^+$ odontoblasts did not express Ki67 in either control or odontoblast-depleted mice, indicating that the odontoblasts were in a quiescent state (Fig. 2D, arrows: Ki67$^-$Col1(2.3)-GFP$^+$ odontoblasts, arrowheads: Ki67$^+$Col1(2.3)-GFP$^-$ dental pulp cells). Consistent with these data, although many EdU$^+$ cells were detected in the marrow spaces of the alveolar bone (Ab), EdU was not incorporated into Col1(2.3)-GFP$^+$ odontoblasts in control mice (Fig. 2E, yellow asterisks: EdU$^+$ cells in Ab, white arrows in square 1: EdU$^-$ Col1(2.3)-GFP$^+$CD45$^-$Ter119$^-$ odontoblasts). Similarly, EdU$^+$ cells were not observed in control pulpal tissue (Fig. 2E, square 2). In contrast, EdU-incorporated Col1(2.3)-GFP$^+$ odontoblast-like cells were observed along the dentin surfaces in odontoblast-depleted molars [EdU$^+$Col1(2.3)-GFP$^+$CD45$^-$Ter119$^-$ odontoblast-like cells: 3.7 ± 0.6 cells per single pulp horn (1.3×10^4 μm^2), n = 3] (Fig. 2E, yellow arrows in square 3). EdU$^+$ cells other than Col1(2.3)-GFP$^+$ odontoblast-like cells were also observed in odontoblast-depleted pulp tissue. EdU$^+$Col1(2.3)-GFP$^-$ cells localized around the dentin were CD45/Ter119-negative pulp stromal cells (Fig. 2E, white arrowheads in square 3). In contrast, EdU$^+$ cells localized far from dentin were detected as CD45/Ter119-positive hematopoietic cells (Fig. 2E, yellow arrowheads in square 4). These findings suggest that pulp stromal odontoblast precursors proliferate in response to odontoblast death and generate odontoblast-like cells.

3.3. Nes-GFP-positive and Nes-GFP-negative pulp cells localized in the CZ differentiate into odontoblast-like cells in response to odontoblast depletion

To characterize the proliferating precursor of odontoblast-like cells, we analyzed the GFP expression pattern of the dental pulp tissue in the maxillary first molars of *Nes-GFP* reporter mice [23,25]. Nes-GFP$^+$ cells were mainly localized in the CZ; however, low levels of GFP were observed in the odontoblast layer (Fig. 3A, white arrows: Nes-

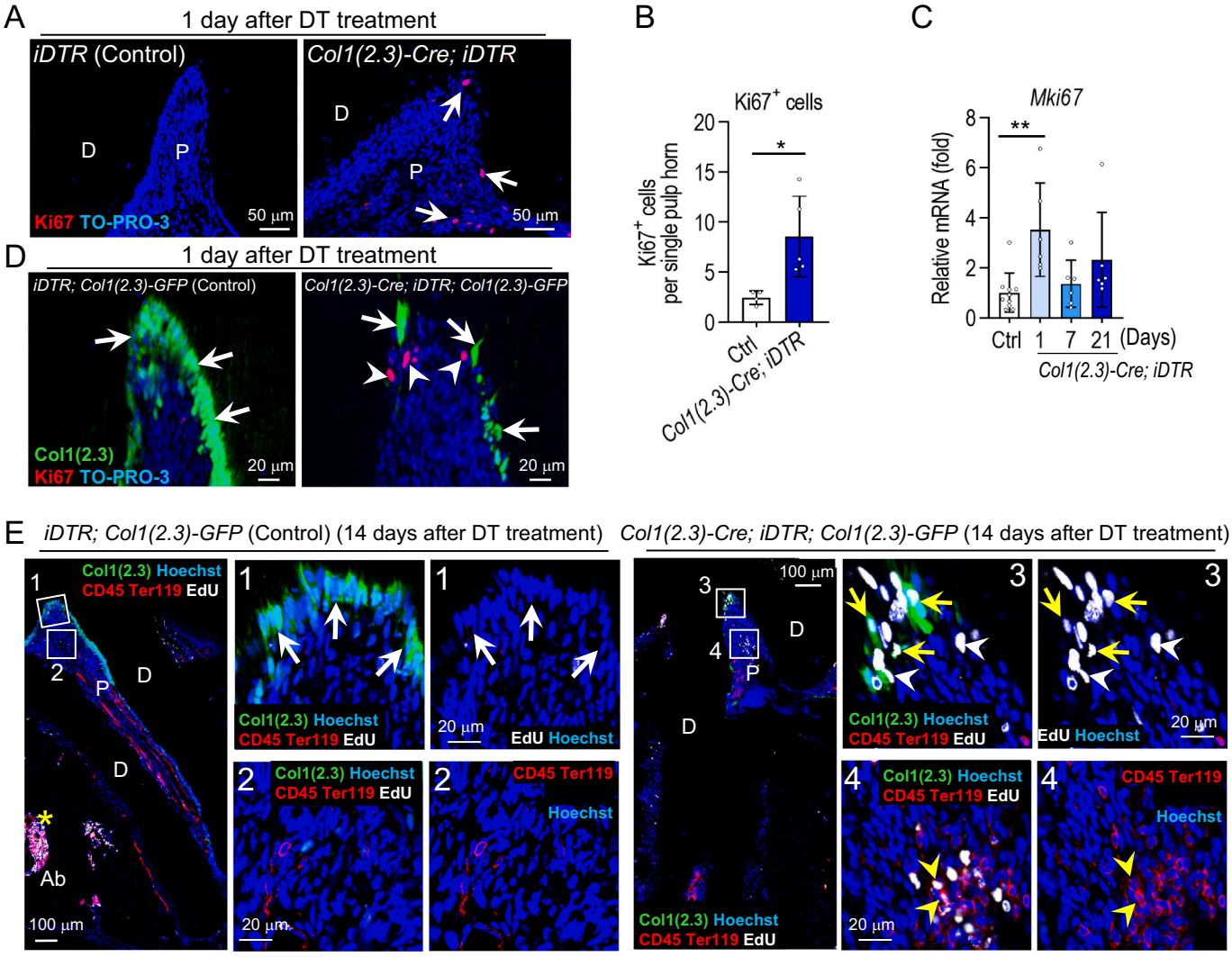

Fig. 2. Dental pulp stromal cells proliferate and differentiate into odontoblast-like cells after odontoblast depletion.
A–E. *Col1(2.3)-Cre; iDTR* and *iDTR* (control) mice (A–C) or *Col1(2.3)-Cre; iDTR; Col1(2.3)-GFP* and *iDTR; Col1(2.3)-GFP* (control) mice (D and E) (all 12 weeks old) were treated with diphtheria toxin (DT) (250 ng/day) for 1 week and analyzed at the indicated time points after the final DT injection. (A and B) Confocal images (A) and quantification (B: 2.0×10^5 μm^2 from the top of a single pulp horn) of Ki67$^+$ cells in thick maxillary first molar (MFM) sections. Arrows: Ki67$^+$ cells. Scale bar = 50 μm. Control: n = 4, *Col1(2.3)-Cre; iDTR*: n = 5. Two-tailed Welch's *t*-test. (C) Real-time PCR for *Mki67* expression in MFMs. Control: n = 10 (10 MFMs), *Col1(2.3)-Cre; iDTR* (day 1): n = 3 (6 MFMs), (day 7): n = 4 (6 MFMs), (day 21): n = 3 (6 MFMs). One-way analysis of variance (ANOVA) followed by Kruskal-Wallis test. (D) Confocal images of Ki67$^+$ cells in thick MFM sections. Arrows: Ki67$^-$Col1(2.3)-GFP$^+$ odontoblasts, arrowheads: Ki67$^+$Col1(2.3)-GFP$^-$ dental pulp cells. Scale bar = 20 μm. Control: n = 4, *Col1(2.3)-Cre; iDTR*: n = 5. (E) One day after the final DT injection, 5-ethynyl-2′-deoxyuridine (EdU) (0.4 mg/day) was injected for 13 days, and imaging analysis was performed on day 14. Confocal images of EdU$^+$ cells in 10-μm-thick MFM sections. White arrows: EdU$^-$Col1(2.3)-GFP$^+$CD45$^-$Ter119$^-$ odontoblasts; asterisks: EdU$^+$ cells in Ab; yellow arrows: EdU$^+$Col1(2.3)-GFP$^+$CD45$^-$Ter119$^-$ odontoblast-like cells; white arrowheads: EdU$^+$Col1(2.3)-GFP$^-$CD45$^-$Ter119$^-$ pulp stromal cells; yellow arrowheads: EdU$^+$Col1(2.3)-GFP$^-$CD45$^+$Ter119$^+$ hematopoietic cells. Scale bar = 100 μm. Numbered panels represent the magnified views of the boxed areas. Scale bar = 20 μm. Control: n = 4, *Col1(2.3)-Cre; iDTR*: n = 3. Nuclei were visualized using TO-PRO-3 (A and D) and Hoechst (E). P: pulp, D: dentin, Ab: alveolar bone, Ctrl: control. *$p < 0.05$, **$p < 0.01$. Data are represented as mean ± standard deviation (SD). (For interpretation of the references to colour in this figure legend, the reader is referred to the web version of this article.)

GFP$^+$αSMA$^-$ cells in the CZ, yellow arrows: Nes-GFP^{low}αSMA$^-$ odontoblasts). CD45/Ter119-positive hematopoietic cells and CD31-positive endothelial cells did not express Nes-GFP, indicating that the Nes-GFP-labeled cells are confined to the pulp stromal population (Fig. 3B and C, arrows: Nes-GFP$^-$CD45$^+$Ter119$^+$ hematopoietic cells, arrowheads: Nes-GFP$^-$CD31$^+$ endothelial cells). Immunofluorescence revealed no overlap between Nes-GFP$^+$ and αSMA$^+$ DPSCs (Fig. 3A, arrowheads: Nes-GFP$^-$αSMA$^+$ DPSCs). In addition, *Nes* mRNA levels decreased on days 1 and 7 after odontoblast depletion but significantly recovered by day 21 (Fig. 3D, left panel). However, *αSma* mRNA was unaffected by odontoblast death (Fig. 3D, right panel). To assess whether Nes-GFP$^+$ cells in the CZ proliferate after odontoblast depletion, we generated *Col1(2.3)-Cre; iDTR; Nes-GFP* mice and administered EdU for 2 weeks post odontoblast depletion. EdU$^+$ nuclei were not observed in Nes-GFP$^+$ cells in the CZ or in αSMA$^+$ DPSCs in the control pulp tissues (Fig. 3E, squares 1 and 2). Importantly, Nes-GFP$^+$ cells in the CZ, but not αSMA$^+$ DPSCs, were detected as EdU$^+$ cells in the odontoblast-depleted pulp tissue (Fig. 3E, white arrows in square 3: EdU$^+$Nes-GFP$^+$αSMA$^-$ cells in the CZ, yellow arrows in square 4: EdU$^-$Nes-GFP$^-$αSMA$^+$ DPSCs, quantification is shown in the left and middle graphs of Fig. 3G). Remarkably, some Nes-GFP-negative cells localized in the CZ were also detected as EdU$^+$ cells (Fig. 3E, arrowheads in square 3). To rule out the possibility that these EdU$^+$Nes-GFP$^-$ cells are hematopoietic cells, sections were further stained with CD45 and Ter119 antibodies (Fig. 3F) to quantify the EdU$^+$Nes-GFP$^-$αSMA$^-$CD45$^-$Ter119$^-$ population; we found that this population was significantly increased upon odontoblast depletion

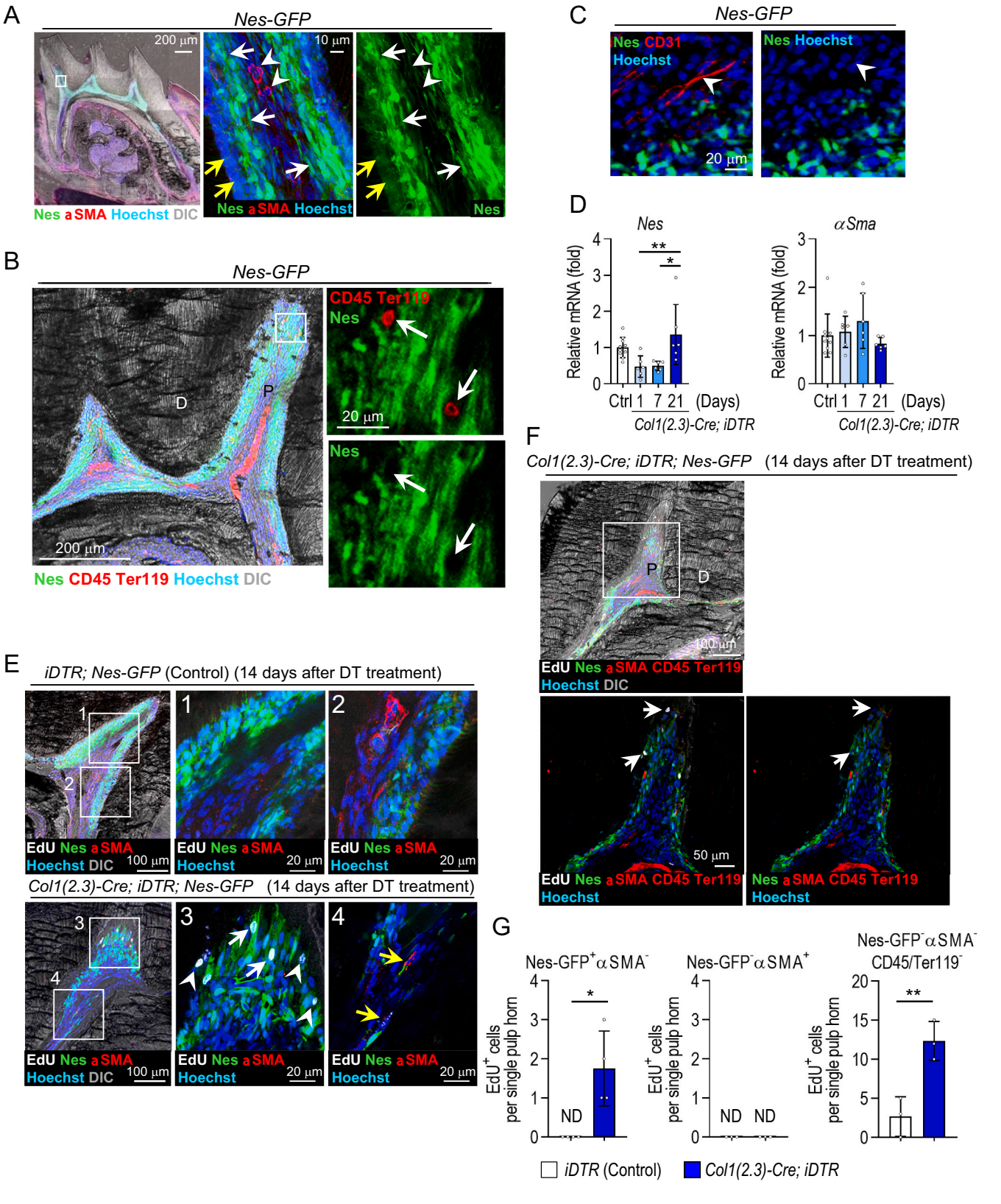

(caption on next page)

Fig. 3. Nes-GFP-positive and Nes-GFP-negative cells localized in the cell-rich zone contribute to odontoblast-like cells after odontoblast depletion.
A–C. Confocal images (Z stack) (A and B, left panel) and confocal images (B, right panels, and C) of thick maxillary first molar (MFM) sections stained with αSMA (A), CD45 and Ter119 (B), or CD31 (C) antibodies from 20-week-old *Nes-GFP* mice. (A) White arrows: Nes-GFP^{+}αSMA^{-} cells in the CZ; yellow arrows: Nes-GFP^{low}αSMA^{-} odontoblasts; arrowheads: Nes-GFP^{-}αSMA^{+} DPSCs. Scale bar = 200 μm. Middle and right panels represent the magnified views of the boxed areas. Scale bar = 10 μm. n = 3. (B) Arrows: Nes-GFP^{-}CD45^{+}Tre119^{+} hematopoietic cells. Scale bar = 200 μm. Right panels are magnified views of the boxed areas. Scale bar = 20 μm. n = 3. (C) Arrowheads: Nes-GFP^{-}CD31^{+} endothelial cells. Scale bar = 20 μm. n = 3. **D–G.** *Col1(2.3)-Cre; iDTR* and *iDTR* (control) mice (D) or *Col1(2.3)-Cre; iDTR; Nes-GFP* and *iDTR; Nes-GFP* (control) mice (E-G) (all 12 weeks old) were treated with diphtheria toxin (DT) (250 ng/day) for 1 week and analyzed at the indicated time points after the final DT injection. (D) Real-time PCR for *Nes* and *αSMA* expression in MFMs. Control: n = 10 (10 MFMs), *Col1(2.3)-Cre; iDTR* (day 1): n = 3 (6 MFMs), (day 7): n = 4 (6 MFMs), (day 21): n = 3 (6 MFMs). One-way analysis of variance (ANOVA) followed by Tukey's test (left panel) and one-way ANOVA followed by Kruskal-Wallis test (right panel). (E–G) One day after the final DT injection, EdU (0.4 mg/day) was injected for 13 days, and the sample was used for imaging analysis on day 14. (E) Confocal images (Z stack) (left panels) and confocal images (middle and right panels) of thick MFM sections stained with αSMA antibody. White arrows: EdU^{+}Nes-GFP^{+}αSMA^{-} cells in the CZ; yellow arrows: EdU^{-}Nes-GFP^{-}αSMA^{+} DPSCs; arrowheads: EdU^{+}Nes-GFP^{-}αSMA^{-} cells in the CZ. Scale bar = 100 μm. Numbered panels represent magnified views of the boxed areas. Scale bar = 20 μm. Control: n = 3, *Col1(2.3)-Cre; iDTR*: n = 3. (F) Confocal images (Z stack) (upper panel) and confocal images (lower panels) stained with αSMA, CD45, and Ter119 antibodies. Arrows: EdU^{+}Nes-GFP^{-} αSMA^{-}CD45^{-}Ter119^{-} cells in the CZ. Scale bar = 100 μm. Lower panels show the magnified view of the boxed area. Scale bar = 50 μm. n = 3. (G) Quantification of EdU^{+}Nes-GFP^{+}αSMA^{-} cells in the CZ, EdU^{+}Nes-GFP^{-}αSMA^{+} DPSCs, and EdU^{+}Nes-GFP^{-}αSMA^{-}CD45^{-}Ter119^{-} cells in the CZ of thick MFM sections (1.2×10^{5} μm^{2} from the top of a single pulp horn). n = 3. Two-tailed Mann-Whitney *U* test (left panel) and Two-tailed Student's *t*-test (right panel). Nuclei were visualized using Hoechst. P: pulp, D: dentin, CZ: cell-rich zone, DIC: differential interference contrast, Ctrl: control. *$p < 0.05$, **$p < 0.01$, ND: not detected. Data are represented as mean ± standard deviation (SD). (For interpretation of the references to colour in this figure legend, the reader is referred to the web version of this article.)

(Fig. 3G, right panel). Collectively, these data suggest that Nes-GFP^{+} and Nes-GFP^{-} cells localized in the CZ proliferate and differentiate into odontoblast-like cells after odontoblast depletion. Moreover, these findings indicate that the proliferation of αSMA^{+} DPSCs might be induced earlier or later in response to odontoblast death, which replenishes CZ-localized Nes-GFP^{+} and Nes-GFP^{-} populations.

3.4. Regenerative odontoblast-like cells mediate reparative dentin formation

To test whether the odontoblast depletion-induced odontoblast-like cells mediate reparative dentin formation, we attempted to detect newly calcified dentin in odontoblast-depleted dental tissue using calcein labeling. Following primary dentinogenesis, mature odontoblasts continue to generate secondary dentin, albeit at a slower rate [41]. Although calcein-labeled hard tissue was observed in 4-week-old dentin, it gradually decreased with age and was hardly detectable in 12-week-old dentin (Fig. 4A, arrows: double-labeled dentin by calcein, arrowheads: single-labeled dentin by calcein, Fig. S1A). Consistent with these data, calcein-labeled dentin was not detected in control mice (*iDTR*) older than 12 weeks; however, in molars, the labeled region was dramatically increased 7 days post odontoblast depletion (Fig. 4B, arrows: double-labeled dentin by calcein, Fig. S1B). μ-CT analyses revealed a significantly increased amount of hard tissue and decreased dental pulp volumes in molars 42 days post odontoblast depletion (Fig. 4, C–G). Odontoblast depletion-induced dentin regeneration was confirmed *via* histological analyses (Fig. 4H, arrows: reparative dentin). These observations indicate that the regenerative odontoblast-like cells, produced in response to odontoblast death, exhibit the capacity to promote reparative dentin formation.

3.5. Odontoblast death induces the expression of odontoblast differentiation- and activation-related genes in the pulp environment

To analyze the effect of odontoblast death on the expression of genes related to odontoblast differentiation and activation in the pulp environment, we carried out transcriptional profiling using RNA-sequencing (RNA-seq). Statistical analysis revealed 660 upregulated and 731 downregulated genes [TPM > 1 in at least one sample, adjusted $p < 0.05$, $|\log_2$ fold change$| \geq 0.5$] in the molars 7 days after odontoblast depletion compared with control molars (Fig. 5A). GO analysis revealed that a set of differentially expressed genes—odontoblast-depleted *versus* control molars—is associated with significantly enriched processes, including extracellular matrix organization, positive regulation of the immune response, blood vessel development, and response to wounding (Fig. 5B, File S1), suggesting the activation of tissue regeneration and reparative dentin formation. To comprehensively analyze whether odontoblast death modified the pulp environment status for reparative dentin formation from inactive to active, we performed a gene set enrichment analysis (GSEA). We found that odontoblast-depleted pulp cells expressed several genes related to extracellular matrix organization and the immune response (Fig. 5, C and D, Tables S3-S6). In odontoblast-depleted molars, the expression of cell cycle indicators (*Mki67*) and several odontoblast differentiation- and activation-related genes was significantly increased, including dental matrix protein 1 (*Dmp1*), *Dspp*, *Col1a1*, *Col1a2*, bone gamma-carboxyglutamate protein (*Bglap/osteocalcin*), *Bglap2*, alkaline phosphatase (*Alpl*), and secreted protein acidic and rich in cysteine (*Sparc/osteonectin*) (Fig. 5, E and F) [42–45]. However, the expression levels of secreted phosphoprotein 1 (*Spp1/osteopontin*), runt-related transcription factor 2 (*Runx2*), and *Sp7/osterix* were comparable with those in the control. Additionally, real-time PCR demonstrated that *Runx2* and *Sp7* expression did not change in odontoblast-depleted molars at any time point (Fig. S3). Consistent with our real-time PCR analysis results shown in Fig. 3D, the mRNA level of the CZ marker *Nes* was decreased, but no effect on the DPSC marker *αSma* was observed in odontoblast-depleted molars at this time point (Fig. 5F).

3.6. Odontoblast depletion increases PTH1R expression in the pulp tissue, thereby driving reparative dentin formation

It has been suggested that PTH1R is expressed in developing dental mesenchymal cells [29,30]. Consistently, immunostaining images of postnatal molars on day 7 showed that PTH1R is expressed in dental follicle cells localized in the upper side of the molars, dental pulp cells, and odontoblasts in the pulp horn (Fig. 6A, black arrows: dental follicle cells, asterisks: dental pulp cells, black arrowheads: odontoblasts). However, PTH1R expression decreased with age and was observed in the periodontal ligament (PDL) in 8-week-old mice, whereas it was absent in dental pulp cells and odontoblasts (Fig. 6B, blue arrowheads: PTH1R^{+} PDL cells). Remarkably, we found that the expression of PTH1R was increased in dental pulp cells and odontoblast-like cells at 7 and 21 days after odontoblast depletion, which was undetectable in control pulp tissue (Fig. 6C, arrows: PTH1R^{+} odontoblast-like cells, asterisks: PTH1R^{+} dental pulp cells). Similarly, the expression of *Pth1r* also increased 7 days after odontoblast depletion, although the mRNA levels returned to control levels on day 21 (Fig. 6D and E, arrows: *Pth1r*$^{+}$ cells; quantification is shown in Fig. 6F). We next analyzed the level of Ser133 phosphorylation in cyclic AMP response element-binding protein (CREB), which acts downstream of the PTH1R/cAMP/protein kinase A signaling pathway in odontoblast-depleted dental pulp tissue [46,47]. The level of pCREB (Ser133) was undetectable in the control pulp tissue. However, it dramatically increased 7 days after odontoblast depletion and showed a trend similar to that observed following PTH1R induction

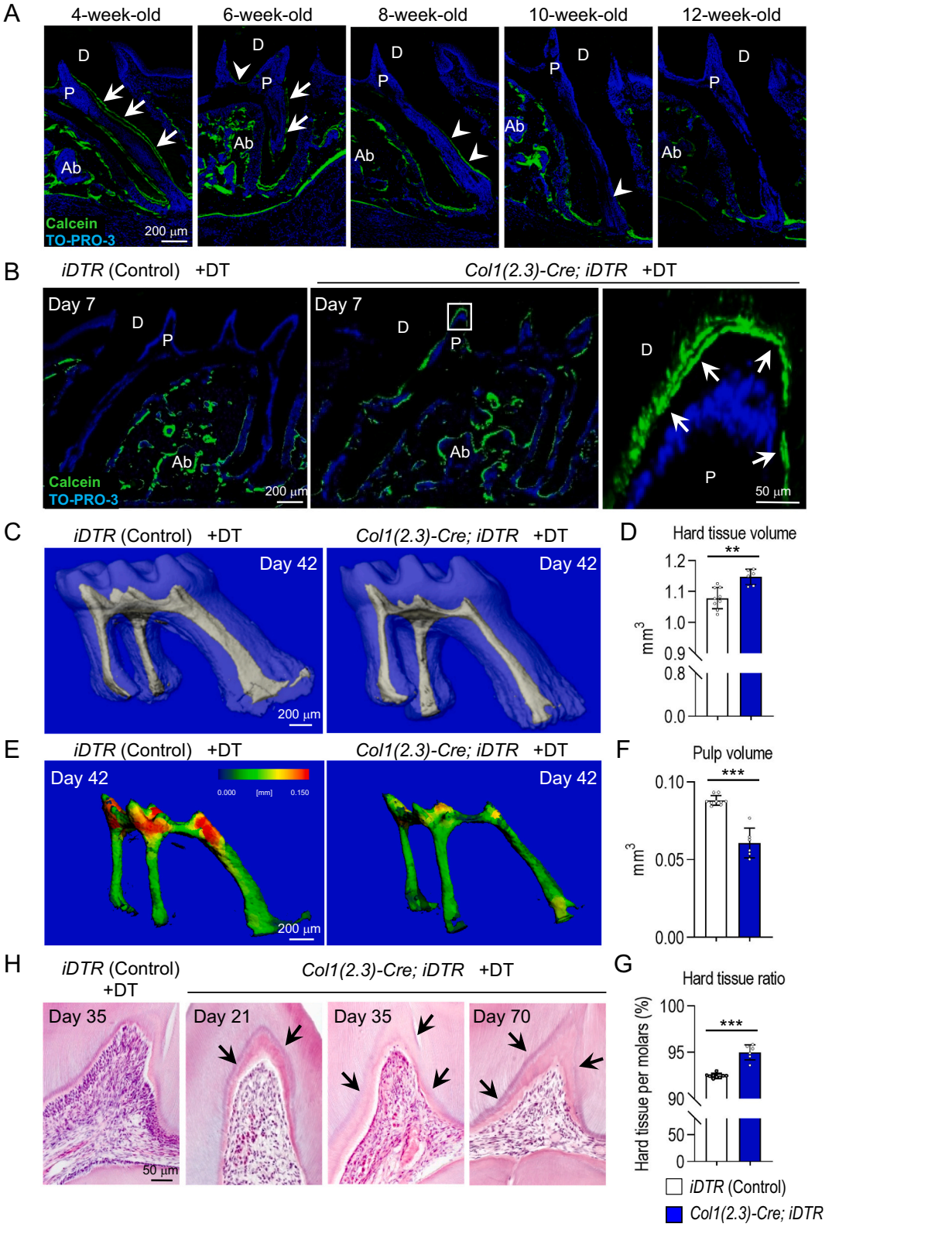

(caption on next page)

Fig. 4. Regenerative odontoblast-like cells induce reparative dentin formation.
A. Confocal images (Z stack) of calcein-labeled thick maxillary first molar (MFM) sections from wild-type mice at indicated stages injected twice with calcein. The second injection was administered 4 days after the first one. Experimental time-course is shown in Fig. S1A. Arrows: calcein double-labeled dentin; arrowheads: calcein single-labeled dentin. Scale bar = 200 μm. n = 3. **B–H.** *Col1(2.3)-Cre; iDTR* and *iDTR* (control) mice (both 12–19 weeks old) were treated with diphtheria toxin (DT) (250 ng/day) for 1 week. (B) Confocal images (Z stack) of thick MFM sections labeled with calcein twice at 3 and 6 days after the final DT injection and analyzed 1 day later. Experimental time-course is shown in Fig. S1B. Arrows: calcein double-labeled dentin. Scale bar = 200 μm. The right panel represents a magnified view of the boxed area. Scale bar = 50 μm. Control: n = 3, *Col1(2.3)-Cre; iDTR*: n = 3. (C–G) Microcomputed tomography (μ-CT) was used to visualize hard tissue and pulp tissue areas (C), and pulp tissue volume (E: heat map indicates the pulp volume) was analyzed 42 days after the final DT injection. Scale bar = 200 μm. Quantification of hard tissue volume (D), pulp volume (F), and hard tissue ratio in the molars (G) was performed. Control: n = 5 (9 MFMs), *Col1(2.3)-Cre; iDTR*: n = 4 (6 MFMs). Two-tailed Student's *t*-test (D), two-tailed Mann-Whitney *U* test (F), and two-tailed Welch's *t*-test (G). (H) Hematoxylin and eosin (HE) staining images showed the area of reparative dentin in MFM sections at the indicated time points after the final DT injection. Scale bar = 50 μm. Control: n = 3, *Col1(2.3)-Cre; iDTR* (day 21–70): n = 4. Arrows: reparative dentin. Nuclei were visualized using TO-PRO-3. P: pulp, D: dentin, Ab: alveolar bone, Ctrl: control. $^{**}p < 0.01$, $^{***}p < 0.001$. Data are represented as mean ± standard deviation (SD).

(Fig. 7A, arrows: pCREB (Ser133)$^+$ dental pulp cells, arrowheads: pCREB (Ser133)$^+$ odontoblast-like cells; quantification of pCREB (Ser133)$^+$ cell frequency in the pulp 7 days after odontoblast depletion is shown in Fig. 7B). The pCREB (Ser133)$^+$ cells were not only observed in the dental pulp tissue but also in the PDL, where PTH1R expression was mainly detected at the adult stage [Fig. 6B, blue arrowheads: PTH1R$^+$ PDL cells; Fig. 7C, asterisks: pCREB (Ser133)$^+$ dental pulp cells, arrows: pCREB (Ser133)$^+$ PDL cells]. These observations suggest that CREB phosphorylation (Ser133) correlates with PTH1R expression.

We next analyzed the levels of *Pthrp*, a ligand of PTH1R, and found comparable mRNA levels between control and odontoblast-depleted molars at any time point (Fig. 8A). It has been demonstrated that PTHrP is mainly expressed in the dental follicle but not in the dental pulp tissue [29]. These findings indicate the possibility that PTH1R induced in odontoblast-depleted molars could be further activated by ligand treatment. To confirm this, we intermittently injected PTH (1–34) (80 μg/kg/12 h) into *Col1(2.3)-Cre; iDTR* mice for 16 days during odontoblast depletion-induced reparative dentin formation (Fig. S1C). Previously, we confirmed that this PTH treatment dose significantly increases bone volume for 10 days [48]. As expected, the calcein labeling experiment demonstrated that reparative dentin formation was significantly accelerated in response to PTH (1–34) treatment in odontoblast-depleted molars [Fig. 8B; quantification of the mineral apposition rate (MAR) is shown in Fig. 8C]. We further examined the effect of PTH (1–34) treatment on the regeneration of odontoblasts using *Col1(2.3)-Cre; iDTR; Col1(2.3)-GFP* mice. In contrast to the positive effect on reparative dentin formation, the number of regenerated Col1 (2.3)-GFP$^+$ odontoblast-like cells were comparable between vehicle and PTH (1–34)-treated mice (Fig. 8, D and E). These observations demonstrate that the PTH/PTH1R signaling cascades are positive regulators of reparative dentin formation but not of odontoblast regeneration in the odontoblast-depleted dental pulp environment.

Finally, we analyzed whether physical pulp-exposed dentin damage-induced odontoblast death activates the PTH1R signaling axis. The pulp-exposed cavity was prepared in mouse maxillary first molars by using a steel bar, and pulp capping was performed using MTA. PTH1R expression was notably increased in the dental pulp cells and in odontoblast-like cells beneath the damaged area after 2 weeks of cavity preparation (Fig. 9A, black arrows: PTH1R$^+$ dental pulp cells, black arrowheads: PTH1R$^+$ odontoblast-like cells). Consistent with the expression pattern of PTH1R, most of the pCREB (Ser133) was also detected near the damaged area [Fig. 9A, red arrows: pCREB (Ser133)$^+$ dental pulp cells, red arrowheads: pCREB (Ser133)$^+$ odontoblast-like cells]. Reparative dentin was observed at 4 weeks after the damage, and the levels of PTH1R and CREB (Ser133) phosphorylation were sustained till this time point (Fig. 9B, asterisks: reparative dentin). These observations indicate that enhanced PTH1R expression and CREB (Ser133) phosphorylation following odontoblast death occurred not only *via* the Cre/LoxP-based strategy but also in response to physical hard tissue defects. We further analyzed whether the physical damage-induced reparative dentin formation is accelerated by PTH treatment. Mice were subjected to pulp-exposed dentin damage, and intermittently injected with PTH (1–34) (80 μg/kg/12 h) (Fig. S1D). Although there was no significant difference, the reparative dentin formation tended to increase with PTH treatment (Fig. 9, C and D). Therefore, we suggest that the PTH1R-mediated signaling cascade may positively regulate reparative dentin formation.

4. Discussion

The immature odontoblast population is believed to contribute to the formation of reparative dentin that will replenish the depleted odontoblasts as a result of severe dental tissue damage; however, this regenerative process is still unclear. Targeted cell depletion approaches using genetically modified mice provide a method to understand the *in vivo* events related to tissue environment modifications, specifically those caused by cell death. Our comprehensive analyses revealed that pulp regeneration could be triggered by odontoblast death without physical dental tissue damage. In response to odontoblast depression, CZ-localized Nes-GFP$^+$ and Nes-GFP$^-$ cells differentiated into odontoblast-like cells with cell-cycle progression and contributed to reparative dentin formation. During this process, pulpal PTH1R expression was increased, and its ligand stimulation accelerated reparative dentin formation (Fig. 10). Furthermore, these data shed light on an unknown regulatory mechanism of dental tissue regeneration mediated by CZ-localized cells.

Our data indicated that odontoblast-like cells were generated from dental pulp cells localized in the CZ in response to odontoblast depletion. The CZ has been considered as a reservoir of odontoblast precursors because it is localized adjacent to the odontoblast layer in the dental pulp tissue. However, the mechanistic details of the differentiation of cells in the CZ into odontoblast-like cells remain unclear. Reportedly, the CZ can be detected through CD90 expression in the rat dental pulp tissue, and a higher calcification activity has been observed in the FACS-sorted CD90$^+$ pulp population than in the CD90$^-$ pulp population, both *in vitro* and *in vivo* [20]. This suggests that the committed odontoblast precursors are localized in the CZ. Moreover, when the rat dental pulp hard tissue was removed and subcutaneously transplanted, calcification was first observed in the pulp cells localized in the CZ [49]. Of note, in the transplanted pulp tissue, the pre-existing odontoblasts were depleted as a result of physical damage. Therefore, consistent with our data, the formation of odontoblast-like cells may have been triggered by odontoblast depletion. These findings suggest that odontoblasts may function as suppressors of the odontoblastogenesis mediated by odontoblast precursors localized in the CZ; however, further studies demonstrating this hypothesis are warranted.

EdU administration demonstrated that Nes-GFP-positive and Nes-GFP-negative cells in the CZ proliferate and differentiate into odontoblast-like cells (Fig. 3). In agreement with previous studies, our data confirmed that Nes-GFP expression decreased through odontoblast differentiation [22] (Fig. 3A). Further, with respect to odontoblastogenesis, the Nes-GFP$^-$ cells may represent a more mature subpopulation than Nes-GFP$^+$ cells in the CZ. Combinations with other reporter murine models that enable monitoring odontoblastogenesis using fluorescence

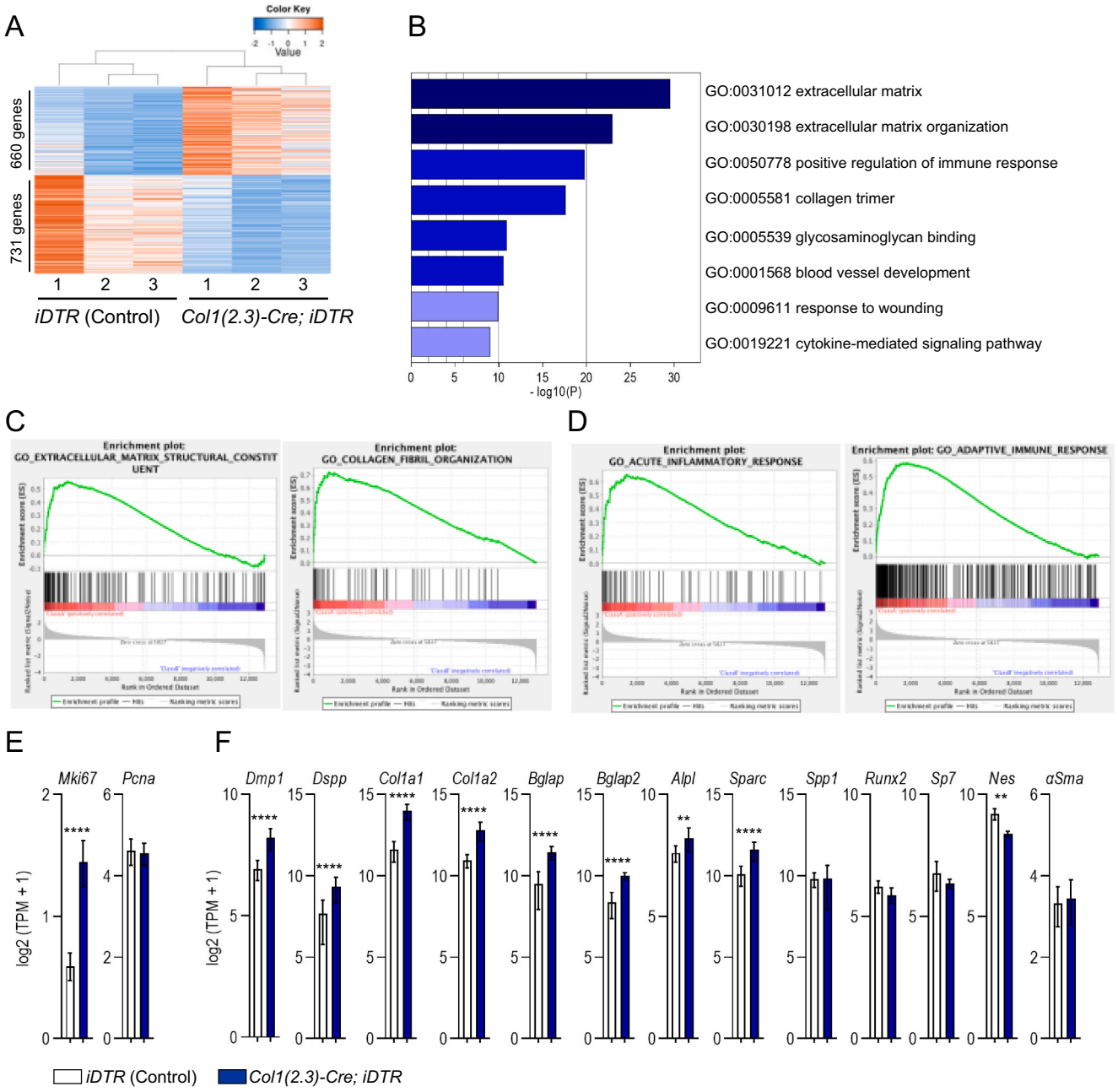

Fig. 5. Odontoblast depletion increases the expression of reparative dentinogenesis-related genes.
A-F. *Col1(2.3)-Cre; iDTR* and *iDTR* (control) mice (both 16–24 weeks old) were administered diphtheria toxin (DT) (250 ng/day) for 1 week; maxillary first molars (MFMs) were used for transcriptional profiling using RNA-sequencing 7 days after the final DT injection [transcript kilobase per million (TPM) > 1 in at least one sample, adjusted $p < 0.05$, | $\log_2$ fold change | ≥0.5]. Control: n = 3, *Col1(2.3)-Cre; iDTR*: n = 3. (A) Heat map showed 660 and 731 genes significantly upregulated and downregulated, respectively, in odontoblast-depleted molars when compared with the control. (B) Gene ontology (GO) analysis showed the biological processes significantly affected by odontoblast depletion in the molars. (C and D) Gene set enrichment analysis (GSEA) showed significant enrichment of genes related to the extracellular matrix structural constituent and collagen fibril organization (C) and acute inflammatory response and adaptive immune response (D). (E and F) The expression of cell cycle-related genes (E) and odontoblast differentiation- and activation-related genes (F) in odontoblast-depleted molars was compared with that in the controls. $^{**}p < 0.01$, $^{****}p < 0.0001$. Data are represented as mean ± standard deviation (SD).

markers besides GFP, such as DSPP-cerulean, may help address this distinction [50].

Previous histological time-course analyses have shown that the odontoblast-like cells differentiated from CZ-localized pulp cells in response to pulp-unexposed mild dental tissue damages, which deplete odontoblasts without causing unrelated pulp cell damage [19]. This report suggests that when the CZ-localized odontoblast precursor pool is undamaged, it provides sufficient odontoblast-like cells to replenish the depleted odontoblast population, and subsequently, CZ-localized odontoblast precursors are replenished by DPSCs. When severe tissue damage depletes not only the odontoblasts but also the CZ-localized pulp cells, lineage contribution of DPSCs might be more prominent than that in the odontoblast depletion mouse model. Targeted cell depletion of Nes^{+} pulp cells in the CZ, as well as odontoblasts, using the *Nes-Cre^{ERT2}; iDTR* mouse model might help demonstrate this hypothesis [24].

It has been suggested that the Wnt signaling cascades positively regulate reparative dentin formation in mouse models of molar tooth

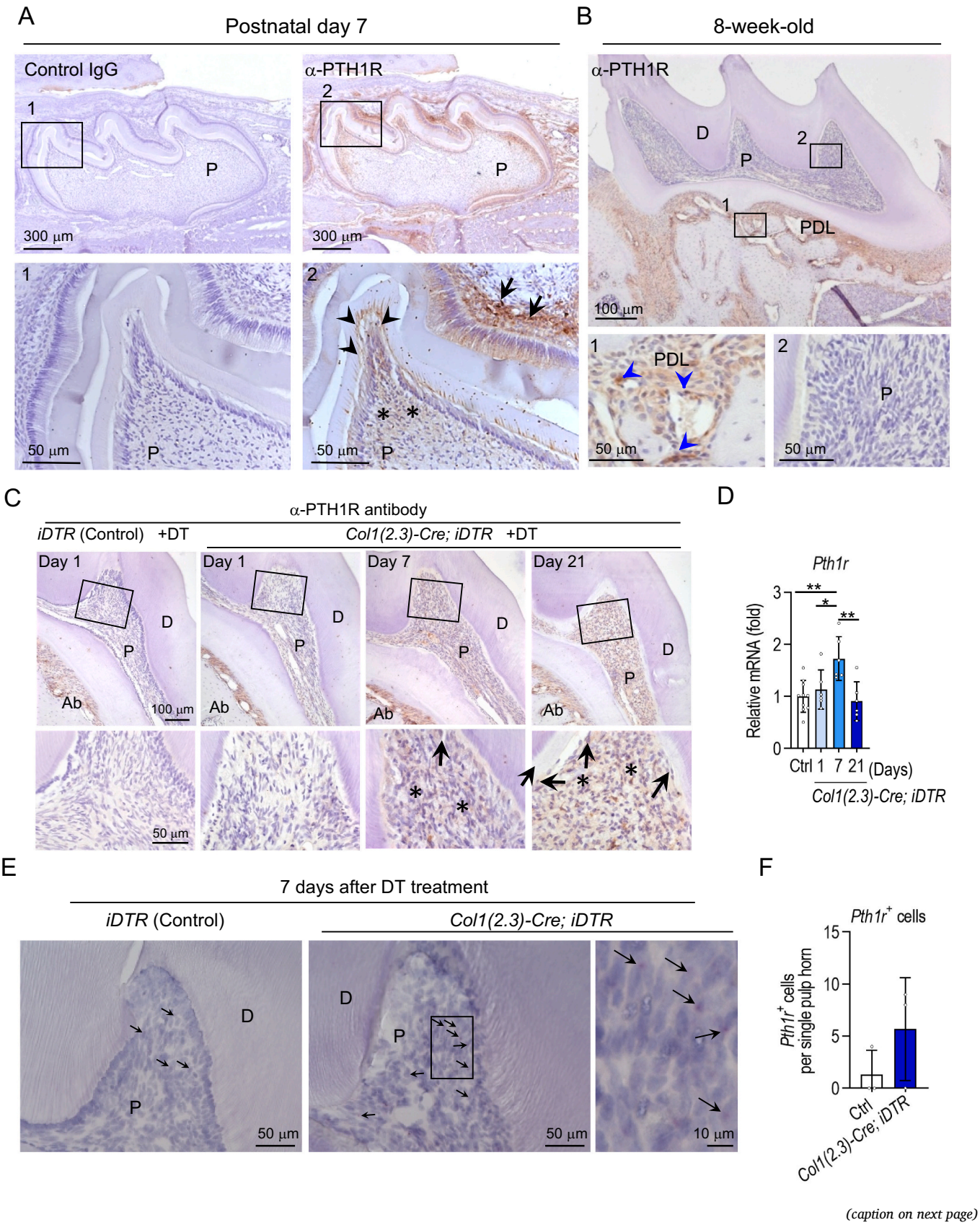

(caption on next page)

Fig. 6. Odontoblast death increases PTH1R levels in the pulp tissue.
A and B. Immunostaining for type I parathyroid hormone receptor (PTH1R)$^+$ cells using an anti-PTH1R antibody in the maxillary first molar (MFM) sections from postnatal day 7 (A) and 8-week-old (B) wild-type mice. (A) Black arrows: PTH1R$^+$ dental follicle cells; asterisks: PTH1R$^+$ dental pulp cells; black arrowheads: PTH1R$^+$ odontoblasts. Left panels show images stained with control rabbit IgG. Scale bar = 300 μm. Numbered panels represent magnified views of boxed areas. Scale bar = 50 μm. n = 3. (B) Blue arrowheads: PTH1R$^+$ PDL cells. Scale bar = 100 μm. Numbered panels represent magnified views of boxed areas. Scale bar = 50 μm. n = 3. **C–F.** *Col1(2.3)-Cre; iDTR* and *iDTR* (control) mice (both 12–16 weeks old) were administered diphtheria toxin (DT) (250 ng/day) for 1 week and analyzed at the indicated time points after the final DT injection. (C) Images of PTH1R$^+$ cells in MFM sections. Arrows: PTH1R$^+$ odontoblast-like cells, asterisks: PTH1R$^+$ dental pulp cells. Scale bar = 100 μm. Lower panels represent magnified views of the boxed areas. Scale bar = 50 μm. Control: n = 3, *Col1(2.3)-Cre; iDTR* (day 1): n = 3, (day 7): n = 3, (day 21): n = 3. (D) Real-time PCR for *Pth1r* expression in the MFMs. Control: n = 10 (10 MFMs), *Col1(2.3)-Cre; iDTR* (day 1): n = 3 (6 MFMs), (day 7): n = 4 (6 MFMs), (day 21): n = 3 (6 MFMs). One-way analysis of variance (ANOVA) followed by Tukey's test. (E and F) *Pth1r*$^+$ cells detected using *in situ* hybridization in maxillary first molar sections (E), and their quantification (F: 1.4 × 10^5 μm^2 of a single pulp horn). Scale bar = 50 μm. Arrows: Pth1r$^+$ cells. The right panel is a magnified view of the boxed area. Scale bar = 10 μm. Control: n = 3, *Col1(2.3)-Cre; iDTR*: n = 3. Two-tailed Mann-Whitney *U* test. P: pulp, D: dentin, PDL: periodontal ligament, Ab: alveolar bone, Ctrl: control. *$p < 0.05$, **$p < 0.01$. Data are represented as mean ± standard deviation (SD). (For interpretation of the references to colour in this figure legend, the reader is referred to the web version of this article.)

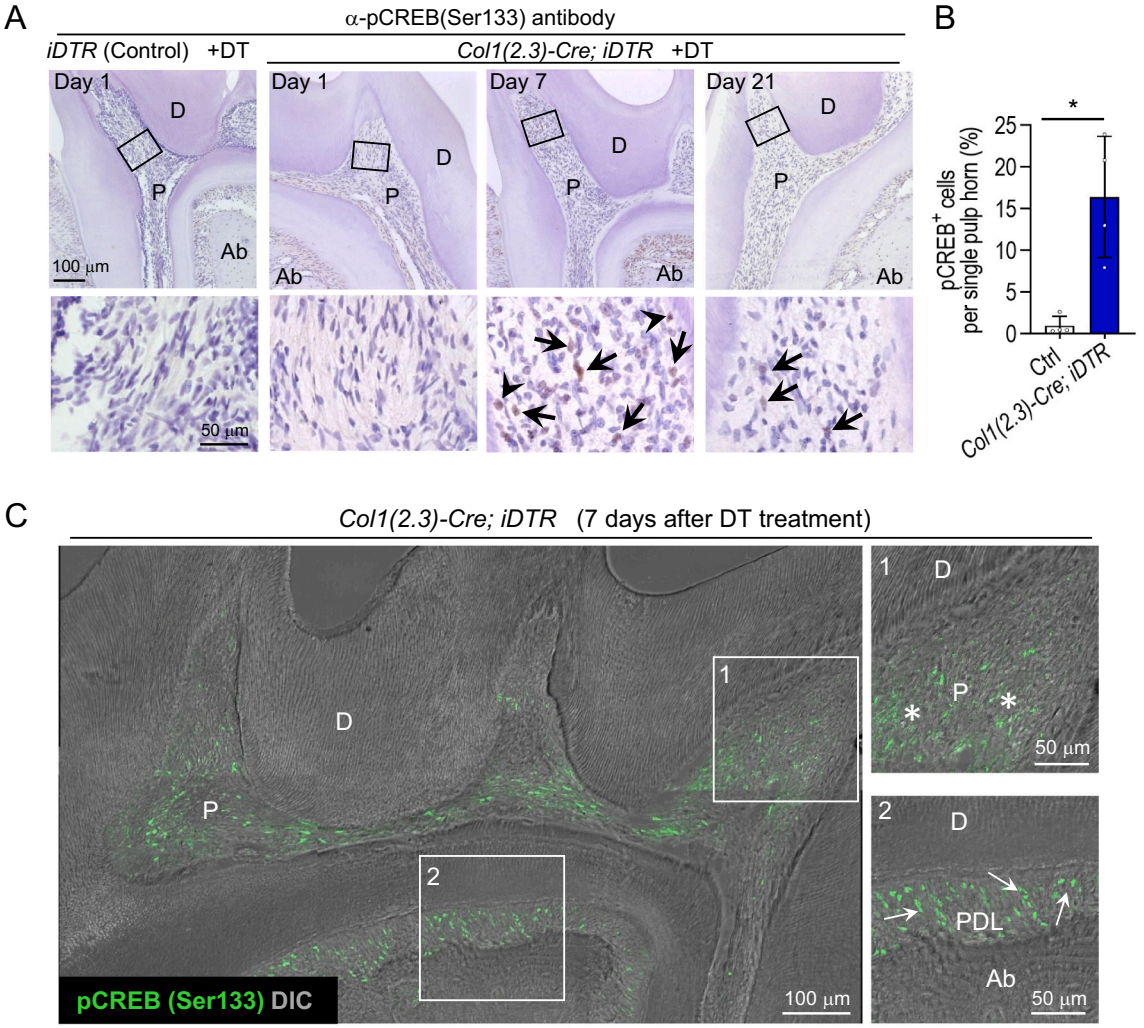

Fig. 7. Odontoblast death increases the levels of the type I parathyroid hormone receptor downstream mediator, pCREB (Ser133), in the pulp tissue.
A–C. *Col1(2.3)-Cre; iDTR* and *iDTR* (control) mice (both 12–16 weeks old) were administered diphtheria toxin (DT) (250 ng/day) for 1 week and analyzed at the indicated time points after the final DT injection. (A and B) Images (A) of cyclic AMP response element-binding protein (pCREB) (Ser133)$^+$ cells in maxillary first molar sections. Arrows: pCREB (Ser133)$^+$ dental pulp cells, arrowheads: pCREB (Ser133)$^+$ odontoblast-like cells. Scale bar = 100 μm. Lower panels represent magnified views of the boxed areas. Scale bar = 50 μm. Control: n = 4, *Col1(2.3)-Cre; iDTR* (day 1): n = 4, (day 7): n = 4, (day 21): n = 4. Quantification (B: 3.5 × 10^4 μm^2 of single pulp horn) of pCREB (Ser133)$^+$ cells (%) in the pulp area of control and *Col1(2.3)-Cre; iDTR* (day 7). Two-tailed Mann-Whitney *U* test. (C) The pCREB (Ser133)$^+$ cells are observed in dental pulp and periodontal ligament (PDL). Scale bar = 100 μm. Arrows: pCREB (Ser133)$^+$ PDL, asterisks: pCREB (Ser133)$^+$ pulp cells. n = 3. Numbered panels are magnified views of boxed areas. Scale bar = 50 μm.

damage [14,51]. However, our RNA-seq data showed that the expression of Wnt-related molecules was not increased in odontoblast-depleted dentin tissue (data not shown). In addition, we did not observe contribution of DPSCs to odontoblast depletion-induced reparative dentin formation in our experimental time course (Fig. 3). These results may indicate that Wnt signal activation is only required for DPSC-dependent lineage differentiation in the regenerative pulp tissue.

The expression of PTH1R was increased in the odontoblast-depleted

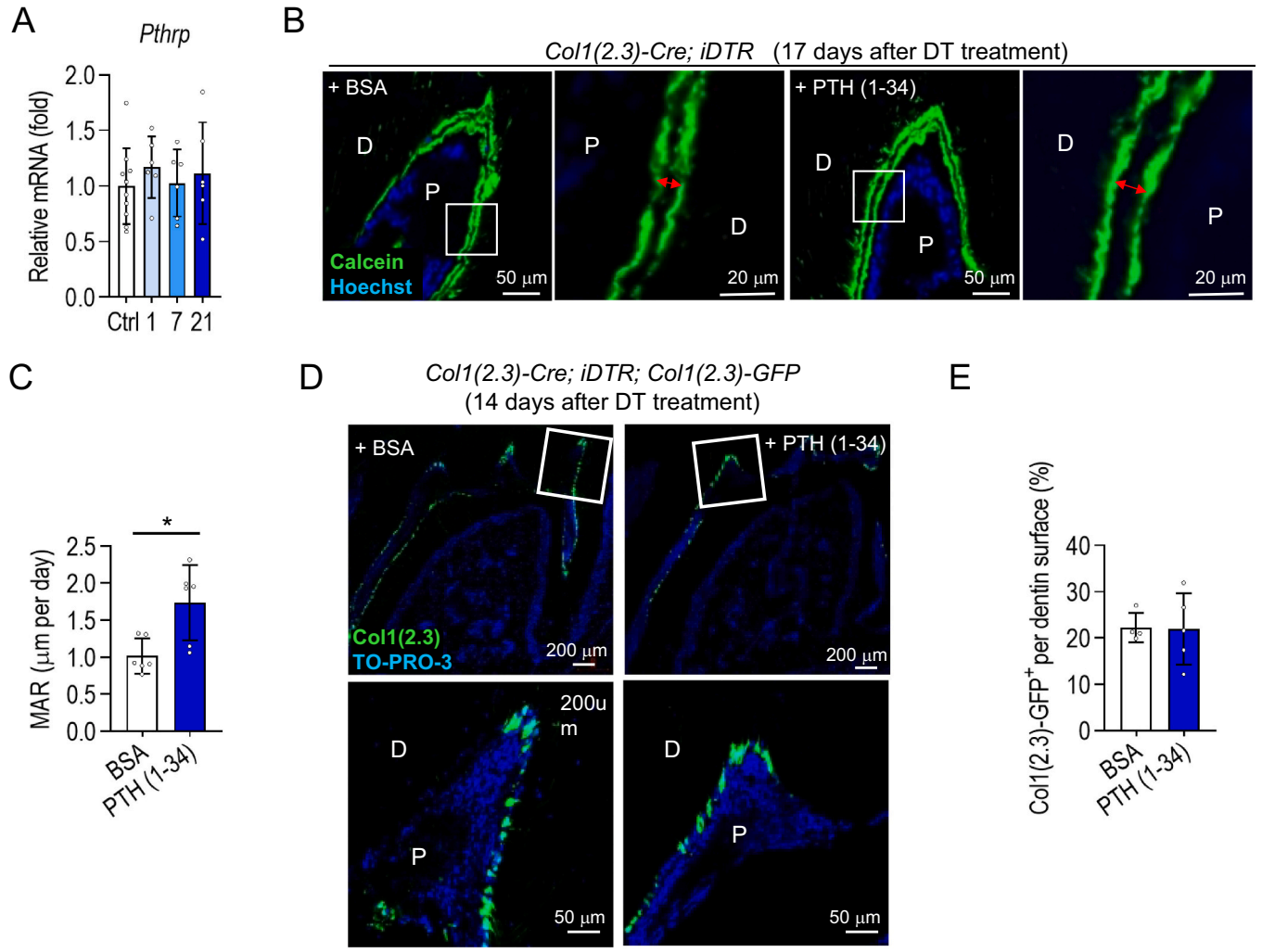

Fig. 8. Exogenous PTH stimulation accelerated dentin formation but not odontoblast regeneration in the odontoblast-depleted dental pulp.
A–E. *Col1(2.3)-Cre; iDTR* and *iDTR* (control) mice (A–C) or *Col1(2.3)-Cre; iDTR; Col1(2.3)-GFP* and *iDTR; Col1(2.3)-GFP* (control) mice (D and E) (both 12–16 weeks old) were treated with diphtheria toxin (DT) (250 ng/day) for 1 week and analyzed at the indicated time points after the final DT injection. (A) Real-time PCR for *Pthrp* expression in the maxillary first molars (MFMs). Control: n = 10 (10 MFMs), *Col1(2.3)-Cre; iDTR* (day 1): n = 3 (6 MFMs), (day 7): n = 4 (6 MFMs), (day 21): n = 3 (6 MFMs). One-way analysis of variance (ANOVA) followed by Tukey's test. (B and C) One day after the final DT injection, parathyroid hormone (PTH) (1–34) (80 μg/kg/12 h) or vehicle (0.1% BSA) was injected for 16 days with calcein labeling on days 11 and 16, and the dentin tissue was used for imaging analysis 1 day after the final calcein injection. Experimental time-course is shown in Fig. S1C. Confocal images (Z stack) of calcein-labeled thick MFM sections (B), Scale bar = 50 μm, and quantification of mineral apposition rate (MAR) (C). Bidirectional arrows: distance between calcein-labeled dentin. Right panels represent the magnified views of the boxed areas. Scale bar = 20 μm. BSA: n = 4 (6 MFMs), PTH: n = 6 (6 MFMs). Two-tailed Student's *t*-test. (D and E) One day after the final DT injection, PTH (1–34) (80 μg/kg/12 h) or vehicle (0.1% BSA) was injected for 14 days, and the dentin tissue was used for imaging analysis after 1 day the final PTH injection. Confocal images (Z stack) (D) and quantification [E: percentage of Col1(2.3)-GFP$^+$ surfaces per dentin surface above the pulp floor] of Col1(2.3)-GFP$^+$ cells in thick MFM sections. Scale bar = 200 μm. Lower panels represent magnified views of the boxed areas. Scale bar = 50 μm. BSA: n = 4, PTH: n = 5. Two-tailed Student's *t*-test. Nuclei were visualized using Hoechst (B) or TO-PRO-3 (D). P: pulp, D: dentin, Ctrl: control, BSA: bovine serum albumin. *$p < 0.05$. Data are represented as mean ± standard deviation (SD).

dental pulp, suggesting that an unknown mediator may regulate this phenomenon in the pulp (Fig. 6, C–F). A previous report revealed that glycoprotein 130 (gp130), a common IL-6 superfamily receptor subunit, is required for PTH1R expression in osteoblast lineages [52]. This report suggested that the gp130-mediated signaling cascade may be a positive regulator of PTH1R expression. Our RNA-seq analysis showed that the *gp130* expression level was not changed by odontoblast depletion (Fig. S4); however, expression of the co-receptors of gp130, oncostatin M receptor (*Osmr*) and IL-27 receptor alpha (*Il27ra*), was significantly increased in response to odontoblast death (Fig. S4). In addition, *Osmr* was identified both with the GO terms "positive regulation of immune response" and "cytokine-mediated signaling pathway" (Fig. 5B, File S1), and in the list of acute inflammatory response-related genes used for GSEA (Fig. 5D, Table S5). Similarly, *Il27ra* was listed with the GO term "positive regulation of immune response" (Fig. 5B, File S1), and with the adaptive immune response-related genes used for GSEA (Fig. 5D, Table S6). These results may suggest that the immunological events are related to the up-regulation of PTH1R in response to odontoblast death. When it comes to another regulatory mechanism, PTH1R expression in the bone tissue has been reported to be suppressed by 1,25-dihydroxyvitamin D3 through the regulation of promoter activity localized in the 5′ untranslated region of exon 3 [53]. This report suggests the possibility that the suppression of the PTH1R pathway is cancelled by the odontoblast-depleted pulp environment; however, further studies are needed to elucidate it.

It has been suggested that PTHrP is not expressed in dental pulp (29), and our data demonstrated that the *Pthrp* expression level is not increased in the odontoblast-depleted pulp tissue. However, PTHrP may

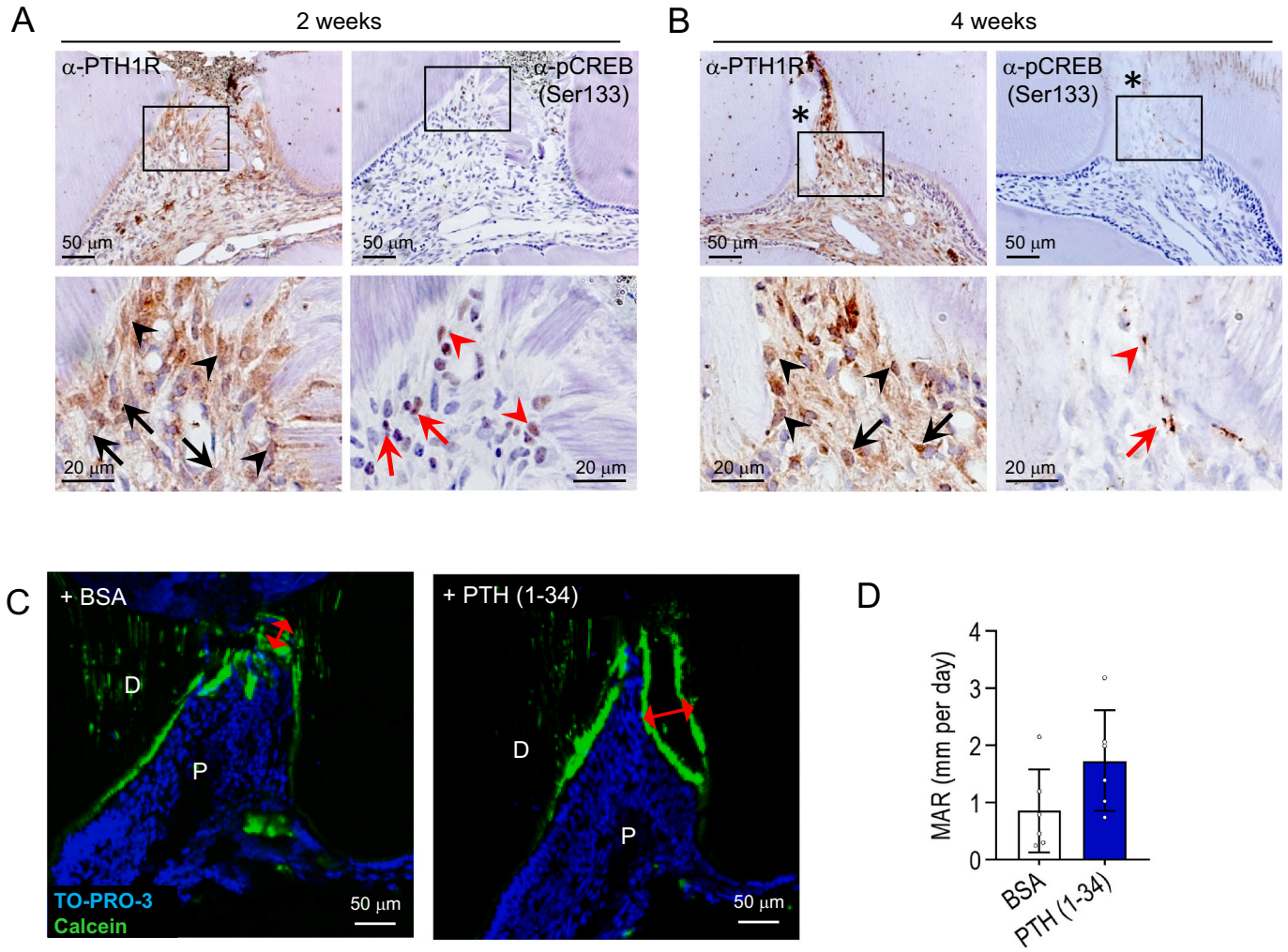

Fig. 9. Levels of PTH1R and pCREB (Ser133) increased in the physically damaged pulp.
A and B. Images of type I parathyroid hormone receptor $(PTH1R)^+$ and cyclic AMP response element-binding protein (pCREB) $(Ser133)^+$ cells in maxillary first molar (MFM) sections 2 (A) and 4 (B) weeks after cavity preparation in 6–12-week-old wild-type mice. Scale bar = 50 μm. Black arrows: $PTH1R^+$ dental pulp cells, black arrowheads: $PTH1R^+$ odontoblast-like cells, red arrows: pCREB $(Ser133)^+$ dental pulp cells; red arrowheads: pCREB $(Ser133)^+$ odontoblast-like cells; asterisks: reparative dentin. Lower panels represent magnified views of the boxed areas. Scale bar = 20 μm. n = 3. **C and D.** After cavity preparation in 12–15-week-old wild-type mice, PTH (1–34) (80 μg/kg/12 h) or vehicle (0.1% BSA) was administered for 12 days, and calcein was administered on days 2 and 12 during the course of PTH treatment; mice were analyzed 1 day after the final calcein injection. Experimental time-course is shown in Fig. S1D. Confocal images (Z stack) of calcein-labeled thick MFM sections (C), Scale bar = 50 μm, and quantification of mineral apposition rate (MAR) (D). Bidirectional arrows: distance between calcein-labeled dentin. BSA: n = 6, PTH: n = 6. Two-tailed Student's *t*-test. Nuclei were visualized using TO-PRO-3. P: pulp, D: dentin, BSA: bovine serum albumin. Data are represented as mean ± standard deviation (SD). (For interpretation of the references to colour in this figure legend, the reader is referred to the web version of this article.)

stimulate PTH1R in the odontoblast-depleted pulp through paracrine action and induce reparative dentin formation. PTH1R- or PTHrP-conditional deletion experiments using *Pth1r-floxed* [54] or *Pthrp-floxed* [55] mice are needed to address this question. Alternatively, this question may be addressed by comparing the dentin calcification activity in organ cultures of odontoblast-depleted molars with and without surrounding dental tissue.

Our data showed that PTH1R expression increased in the dental pulp cells as well as in odontoblast-like cells in odontoblast-depleted molars, suggesting that PTH (1–34) may affect both types of cells (Fig. 6C); however, PTH (1–34) accelerated the reparative dentin formation, but not the odontoblast differentiation in odontoblast-depleted molars (Fig. 8, B–E). Regarding bone formation, previous studies have shown that PTH (1–34) treatment induced differentiation of BM-MSPC into osteoblasts, ultimately resulting in increased bone volume [28,48]. These results indicate that the mechanistic regulation of the formation of PTH-induced hard tissues is different between dentin and bone tissues.

Additionally, increased levels of PTH1R and its downstream signaling molecules—pCREB (Ser133)—were observed in the pulp-exposed mouse molars with prepared cavities and PTH (1–34) treatment tended to increase reparative dentin formation (Fig. 9). These data suggest that the PTH signaling cascade may contribute to reparative dentin formation after cavity preparation in the dentin tissue. We attempted to confirm the significance of CREB activation for odontoblast death-induced reparative dentin formation using the CREB inhibitor, 666-15 [56]. However, the activated pulpal CREB in the odontoblast-depleted pulp tissue was not suppressed by a nonlethal dose of 666-15 (data not shown). In the future, additional studies will be carried out to clarify whether CREB activation is indispensable for reparative dentin formation after odontoblast death. Moreover, future investigations are required to characterize how odontoblast death shapes the dental pulp niche and uncover the underlying network of regulatory mechanisms. Such an approach will enable the clinical applications of PTH (1–34) for dental treatment.

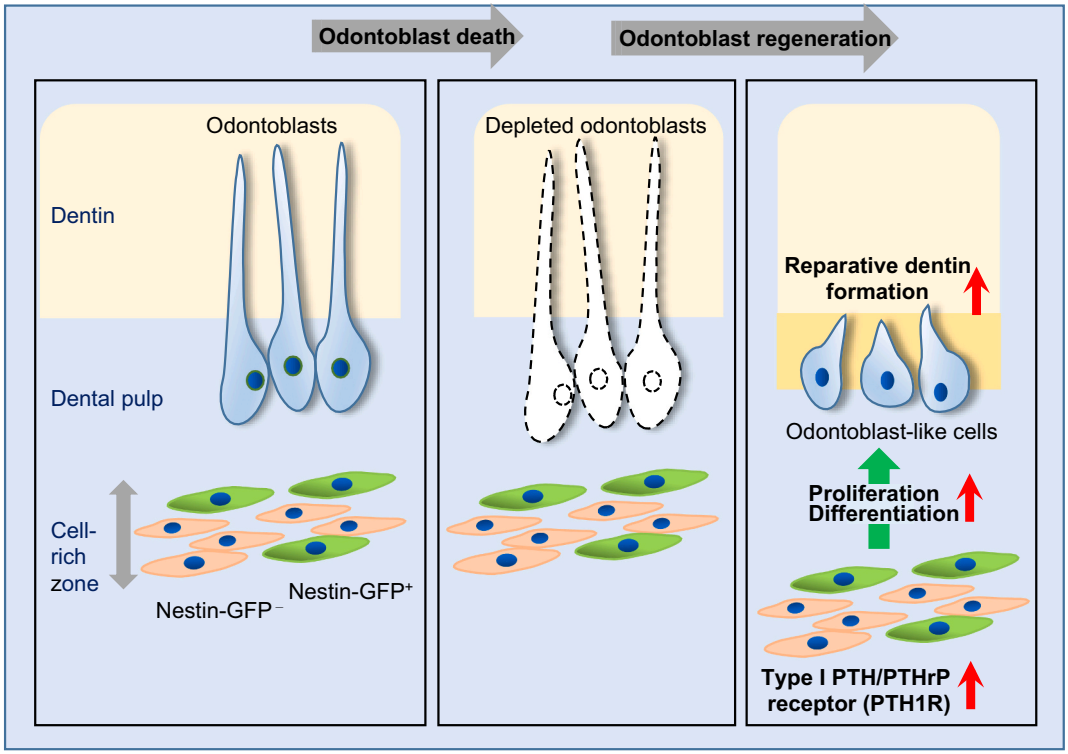

Fig. 10. Effect of odontoblast depletion on the dental pulp environment.
In response to odontoblast depression, Nes-GFP^{+} and Nes-GFP^{-} cells, localized in the cell-rich zone, differentiate into odontoblast-like cells through cell-cycle progression and contribute to reparative dentin formation. PTH1R expression was increased in the odontoblast-depleted pulp tissue, and its ligand stimulation accelerated reparative dentin formation.

5. Conclusion

In conclusion, while our study demonstrates that the activation of the PTH1R signaling cascade positively regulates reparative dentin formation, the mediators of the upregulation of PTH1R in response to Cre/LoxP-mediated odontoblast death or physical pulp-exposed dentin damage remain to be elucidated. Furthermore, it is still unclear whether the upregulation of PTH1R is also induced in damaged dental pulp tissue in humans. In addition, it is necessary to evaluate the age or sex differences in the regeneration of dental tissues. Regardless, our data provide evidence of reparative dentin tissue formation—mediated by CZ-localized cells—in Cre/LoxP-induced odontoblast depletion as well as physical pulp-exposed hard tissue damage.

Data availability

RNA-sequencing data that support the findings of this study have been deposited in the DDBJ Sequenced Read Archive under the accession number DRA010453.

CRediT authorship contribution statement

Lijuan Zhao: Formal analysis, Investigation, Methodology, Visualization, Writing – review & editing. **Shinichirou Ito:** Investigation, Visualization. **Atsushi Arai:** Investigation. **Nobuyuki Udagawa:** Investigation. **Kanji Horibe:** Investigation, Methodology. **Miroku Hara:** Investigation, Methodology, Visualization. **Daisuke Nishida:** Investigation. **Akihiro Hosoya:** Methodology. **Rinya Masuko:** Investigation, Methodology, Visualization. **Koji Okabe:** Investigation. **Masashi Shin:** Investigation, Visualization. **Xianqi Li:** Investigation. **Koichi Matsuo:** Resources. **Shinichi Abe:** Investigation. **Satoru Matsunaga:** Investigation. **Yasuhiro Kobayashi:** Investigation. **Hideaki Kagami:** Investigation. **Toshihide Mizoguchi:** Conceptualization, Formal analysis, Funding acquisition, Investigation, Project administration, Supervision, Visualization, Writing – original draft, Writing – review & editing.

Declaration of competing interest

R.M. is an employee of JEOL Ltd., Tokyo, Japan. All other authors declare that they have no conflicts of interest with the contents of this article.

Acknowledgments

We would like to thank Asahi Kasei Pharma Corporation (Tokyo, Japan) for providing human PTH (1–34) and G. Enikolopov (Stony Brook University, Stony Brook, NY) for the *Nes-GFP* mice. We would also like to thank N. Takahashi (Matsumoto Dental University, Nagano, Japan), A. Yamaguchi (Tokyo Dental College, Tokyo, Japan), and R. Takao-Kawabata (Asahi Kasei Pharma Corporation) for useful advice and comments regarding our work. We appreciate the technical assistance provided by Y. Jing, Y. Mengyu, and H. Zhifeng.

Funding

This work was supported by Grants-in-Aid from the Japan Society for the Promotion of Science (JSPS) KAKENHI (20H03853 and 17H04374 to T.M.), Private University Branding Project of Ministry of Education, Culture, Sports, Science and Technology (MEXT), Japan: Tokyo Dental College Branding Project for Multidisciplinary Research Center for Jaw Disease (MRCJD) (T.M.), The Science Research Promotion Fund from PMAC (T.M.), Takeda Science Foundation (T.M.), and The JSBMR Frontier Scientist Grant (T.M.).

Appendix A. Supplementary data

Supplementary data to this article can be found online at https://doi.org/10.1016/j.bone.2021.116010.

References

[1] T. Suda, N. Takahashi, N. Udagawa, E. Jimi, M.T. Gillespie, T.J. Martin, Modulation of osteoclast differentiation and function by the new members of the tumor necrosis factor receptor and ligand families, Endocr. Rev. 20 (1999) 345–357, https://doi.org/10.1210/edrv.20.3.0367.

[2] W.J. Boyle, W.S. Simonet, D.L. Lacey, Osteoclast differentiation and activation, Nature 423 (2003) 337342, https://doi.org/10.1038/nature01658.

[3] D. Park, J.A. Spencer, B.I. Koh, T. Kobayashi, J. Fujisaki, T.L. Clemens, C.P. Lin, H. M. Kronenberg, D.T. Scadden, Endogenous bone marrow MSCs are dynamic, fate-restricted participants in bone maintenance and regeneration, Cell Stem Cell 10 (2012) 259–272, https://doi.org/10.1016/j.stem.2012.02.003.

[4] T. Mizoguchi, S. Pinho, J. Ahmed, Y. Kunisaki, M. Hanoun, A. Mendelson, N. Ono, H.M. Kronenberg, P.S. Frenette, Osterix marks distinct waves of primitive and definitive stromal progenitors during bone marrow development, Dev. Cell 29 (2014) 340–349, https://doi.org/10.1016/j.devcel.2014.03.013.

[5] N. Ono, W. Ono, T. Nagasawa, H.M. Kronenberg, A subset of chondrogenic cells provides early mesenchymal progenitors in growing bones, Nat. Cell Biol. 16 (2014) 1157–1167, https://doi.org/10.1038/ncb3067.

[6] B.O. Zhou, R. Yue, M.M. Murphy, J.G. Peyer, S.J. Morrison, Leptin-receptor-expressing mesenchymal stromal cells represent the main source of bone formed by adult bone marrow, Cell Stem Cell 15 (2014) 154–168, https://doi.org/10.1016/j.stem.2014.06.008.

[7] M. Nakashima, A.H. Reddi, The application of bone morphogenetic proteins to dental tissue engineering, Nat. Biotechnol. 21 (2003) 1025–1032, https://doi.org/10.1038/nbt864.

[8] Y.D. Zhang, Z. Chen, Y.Q. Song, C. Liu, Y.P. Chen, Making a tooth: growth factors, transcription factors, and stem cells, Cell Res. 15 (2005) 301–316, https://doi.org/10.1038/sj.cr.7290299.

[9] P.T. Sharpe, Dental mesenchymal stem cells, Development 143 (2016) 2273–2280, https://doi.org/10.1242/dev.134189.

[10] J. Feng, A. Mantesso, C. De Bari, A. Nishiyama, P.T. Sharpe, Dual origin of mesenchymal stem cells contributing to organ growth and repair, Proc. Natl. Acad. Sci. U. S. A. 108 (2011) 6503–6508, https://doi.org/10.1073/pnas.1015449108.

[11] H. Zhao, J. Feng, K. Seidel, S. Shi, O. Klein, P. Sharpe, Y. Chai, Secretion of shh by a neurovascular bundle niche supports mesenchymal stem cell homeostasis in the adult mouse incisor, Cell Stem Cell 14 (2014) 160–173, https://doi.org/10.1016/j.stem.2013.12.013.

[12] N. Kaukua, M.K. Shahidi, C. Konstantinidou, V. Dyachuk, M. Kaucka, A. Furlan, Z. An, L. Wang, I. Hultman, L. Ährlund-Richter, H. Blom, Glial origin of mesenchymal stem cells in a tooth model system, Nature 513 (2014) 551–554, https://doi.org/10.1038/nature13536.

[13] I. Vidovic, A. Banerjee, R. Fatahi, B.G. Matthews, N.A. Dyment, I. Kalajzic, M. Mina, αSMA-expressing perivascular cells represent dental pulp progenitors in vivo, J. Dent. Res. 96 (2017) 323–330, https://doi.org/10.1177/0022034516678208.

[14] R. Babb, D. Chandrasekaran, V. Carvalho Moreno Neves, P.T. Sharpe, Axin2-expressing cells differentiate into reparative odontoblasts via autocrine Wnt/β-catenin signaling in response to tooth damage, Sci. Rep. 7 (2017) 3102, https://doi.org/10.1038/s41598-017-03145-6.

[15] A. Nanci, Ten Cate's Oral Histology: Development, Structure, and Function, eighth ed., Elsevier, St. Louis, MO, 2013.

[16] K. Saito, M. Nakatomi, H. Ohshima, Dynamics of bromodeoxyuridine label-retaining dental pulp cells during pulpal healing after cavity preparation in mice, J. Endod. 39 (2013) 1250–1255, https://doi.org/10.1016/j.joen.2013.06.017.

[17] Z. An, M. Sabalic, R.F. Bloomquist, T.E. Fowler, T. Streelman, P.T. Sharpe, A quiescent cell population replenishes mesenchymal stem cells to drive accelerated growth in mouse incisors, Nat. Commun. 9 (2018) 378, https://doi.org/10.1038/s41467-017-02785-6.

[18] J.V. Ruch, H. Lesot, C. Bègue-Kirn, Odontoblast differentiation, Int. J. Dev. Biol. 39 (1995) 51–68.

[19] M. Harada, S. Kenmotsu, N. Nakasone, K. Nakakura-Ohshima, H. Ohshima, Cell dynamics in the pulpal healing process following cavity preparation in rat molars, Histochem. Cell Biol. 130 (2008) 773–783, https://doi.org/10.1007/s00418-008-0438-3.

[20] A. Hosoya, T. Hiraga, T. Ninomiya, A. Yukita, K. Yoshiba, N. Yoshiba, M. Takahashi, S. Ito, H. Nakamura, Thy-1-positive cells in the subodontoblastic layer possess high potential to differentiate into hard tissue-forming cells, Histochem. Cell Biol. 137 (2012) 733–742, https://doi.org/10.1007/s00418-012-0928-1.

[21] N.S. Roy, S. Wang, L. Jiang, J. Kang, A. Benraiss, C. Harrison-Restelli, R.A. Fraser, W.T. Couldwell, A. Kawaguchi, H. Okano, M. Nedergaard, In vitro neurogenesis by progenitor cells isolated from the adult human hippocampus, Nat. Med. 6 (2000) 271–277, https://doi.org/10.1038/73119.

[22] M. Nakatomi, A. Quispe-Salcedo, M. Sakaguchi, H. Ida-Yonemochi, H. Okano, H. Ohshima, Nestin expression is differently regulated between odontoblasts and the subodontoblastic layer in mice, Histochem. Cell Biol. 149 (2018) 383–391, https://doi.org/10.1007/s00418-018-1651-3.

[23] J.L. Mignone, V. Kukekov, A.S. Chiang, D. Steindler, G. Enikolopov, Neural stem and progenitor cells in nestin-GFP transgenic mice, J. Comp. Neurol. 469 (2004) 311–324, https://doi.org/10.1002/cne.10964.

[24] S. Méndez-Ferrer, T.V. Michurina, F. Ferraro, A.R. Mazloom, B.D. Macarthur, S. A. Lira, D.T. Scadden, A. Ma'ayan, G.N. Enikolopov, P.S. Frenette, Mesenchymal and haematopoietic stem cells form a unique bone marrow niche, Nature 466 (2010) 829–834, https://doi.org/10.1038/nature09262.

[25] J. Mignone, N. Peunova, G. Enikolopov, Nestin-based reporter transgenic mouse lines, Methods Mol. Biol. 1453 (2016) 7–14, https://doi.org/10.1007/978-1-4939-3786-8_2.

[26] D.H. Balani, N. Ono, H.M. Kronenberg, Parathyroid hormone regulates fates of murine osteoblast precursors in vivo, J. Clin. Invest. 127 (2017) 3327–3338, https://doi.org/10.1172/JCI91699.

[27] Y. Fan, J.I. Hanai, P.T. Le, R. Bi, D. Maridas, V. DeMambro, C.A. Figueroa, S. Kir, X. Zhou, M. Mannstadt, R. Baron, Parathyroid hormone directs bone marrow mesenchymal cell fate, Cell Metab. 25 (2017) 661–672, https://doi.org/10.1016/j.cmet.2017.01.001.

[28] M. Yang, A. Arai, N. Udagawa, L. Zhao, D. Nishida, K. Murakami, T. Hiraga, R. Takao-Kawabata, K. Matsuo, T. Komori, Y. Kobayashi, Parathyroid hormone shifts cell fate of a leptin receptor-marked stromal population from adipogenic to osteoblastic lineage, J. Bone Miner. Res. 34 (2019) 1952–1963, https://doi.org/10.1002/jbmr.3811.

[29] W. Ono, N. Sakagami, S. Nishimori, N. Ono, H.M. Kronenberg, Parathyroid hormone receptor signalling in osterix-expressing mesenchymal progenitors is essential for tooth root formation, Nat. Commun. 7 (2016) 11277, https://doi.org/10.1038/ncomms11277.

[30] A. Takahashi, M. Nagata, A. Gupta, Y. Matsushita, T. Yamaguchi, K. Mizuhashi, K. Maki, A.C. Ruellas, L.S. Cevidanes, H.M. Kronenberg, N. Ono, Autocrine regulation of mesenchymal progenitor cell fates orchestrates tooth eruption, Proc. Natl. Acad. Sci. U. S. A. 116 (2019) 575–580, https://doi.org/10.1073/pnas.1810200115.

[31] R. Dacquin, M. Starbuck, T. Schinke, G. Karsenty, Mouse alpha1(I)-collagen promoter is the best known promoter to drive efficient Cre recombinase expression in osteoblast, Dev. Dyn. 224 (2002) 245–251, https://doi.org/10.1002/dvdy.10100.

[32] K. Matsuo, Y. Kuroda, N. Nango, K. Shimoda, Y. Kubota, M. Ema, L. Bakiri, E. F. Wagner, Y. Takeda, W. Yashiro, A. Momose, Osteogenic capillaries orchestrate growth plate-independent ossification of the malleus, Development 142 (2015) 3912–3920, https://doi.org/10.1242/dev.123885.

[33] T. Kawamoto, M. Shimizu, A method for preparing 2- to 50-micron-thick fresh-frozen sections of large samples and undecalcified hard tissues, Histochem. Cell Biol. 113 (2000) 331–339, https://doi.org/10.1007/s004180000149.

[34] A. Dobin, C.A. Davis, F. Schlesinger, J. Drenkow, C. Zaleski, S. Jha, P. Batut, M. Chaisson, T.R. Gingeras, STAR: ultrafast universal RNA-seq aligner, Bioinformatics 29 (2013) 15–21, https://doi.org/10.1093/bioinformatics/bts635.

[35] B. Li, C.N. Dewey, RSEM: accurate transcript quantification from RNA-Seq data with or without a reference genome, BMC Bioinform. 12 (2011) 323, https://doi.org/10.1186/1471-2105-12-323.

[36] M.D. Robinson, D.J. McCarthy, G.K. Smyth, edgeR: a Bioconductor package for differential expression analysis of digital gene expression data, Bioinformatics 26 (2010) 139–140, https://doi.org/10.1093/bioinformatics/btp616.

[37] Y. Benjamini, Y. Hochberg, Controlling the false discovery rate: a practical and powerful approach to multiple testing, J. R. Stat. Soc. B 57 (1995) 289–300. http://www.jstor.org/stable/2346101.

[38] Y. Zhou, B. Zhou, L. Pache, M. Chang, A.H. Khodabakhshi, O. Tanaseichuk, C. Benner, S.K. Chanda, Metascape provides a biologist-oriented resource for the analysis of systems-level datasets, Nat. Commun. 10 (2019) 1523, https://doi.org/10.1038/s41467-019-09234-6.

[39] A. Subramanian, P. Tamayo, V.K. Mootha, S. Mukherjee, B.L. Ebert, M.A. Gillette, A. Paulovich, S.L. Pomeroy, T.R. Golub, E.S. Lander, J.P. Mesirov, Gene set enrichment analysis: a knowledge-based approach for interpreting genome-wide expression profiles, Proc. Natl. Acad. Sci. U. S. A. 102 (2005) 15545–15550, https://doi.org/10.1073/pnas.0506580102.

[40] J. Rossert, H. Eberspaecher, B. de Crombrugghe, Separate cis-acting DNA elements of the mouse pro-alpha 1(I) collagen promoter direct expression of reporter genes to different type I collagen-producing cells in transgenic mice, J. Cell Biol. 129 (1995) 1421–1432, https://doi.org/10.1083/jcb.129.5.1421.

[41] A.J. Sloan, A.J. Smith, Stem cells and the dental pulp: potential roles in dentine regeneration and repair, Oral Dis. 13 (2007) 151–157, https://doi.org/10.1111/j.1601-0825.2006.01346.x.

[42] W.T. Butler, H. Ritchie, The nature and functional significance of dentin extracellular matrix proteins, Int. J. Dev. Biol. 39 (1995) 169–179.

[43] P.W. Holland, S.J. Harper, J.H. McVey, B.L. Hogan, In vivo expression of mRNA for the Ca++-binding protein SPARC (osteonectin) revealed by in situ hybridization, J. Cell Biol. 105 (1987) 473–482, https://doi.org/10.1083/jcb.105.1.473.

[44] S. Chen, J. Gluhak-Heinrich, Y.H. Wang, Y.M. Wu, H.H. Chuang, L. Chen, G. H. Yuan, J. Dong, I. Gay, M. MacDougall, Runx2, osx, and dspp in tooth development, J. Dent. Res. 88 (2009) 904–909, https://doi.org/10.1177/0022034509342873.

[45] K. Narayanan, R. Srinivas, A. Ramachandran, J. Hao, B. Quinn, A. George, Differentiation of embryonic mesenchymal cells to odontoblast-like cells by overexpression of dentin matrix protein 1, Proc. Natl. Acad. Sci. U. S. A. 98 (2001) 4516–4521, https://doi.org/10.1073/pnas.081075198.

[46] G.A. Gonzalez, M.R. Montminy, Cyclic AMP stimulates somatostatin gene transcription by phosphorylation of CREB at serine 133, Cell 59 (1989) 675–680, https://doi.org/10.1016/0092-8674(89)90013-5.

[47] T.J. Gardella, J.P. Vilardaga, International Union of Basic and Clinical Pharmacology. XCIII. The parathyroid hormone receptors–family B G protein-coupled receptors, Pharmacol. Rev. 67 (2015) 310–337, https://doi.org/10.1124/pr.114.009464.

[48] M. Yang, A. Arai, N. Udagawa, T. Hiraga, Z. Lijuan, S. Ito, T. Komori, T. Moriishi, K. Matsuo, K. Shimoda, A.H. Zahalka, Osteogenic factor Runx2 marks a subset of leptin receptor-positive cells that sit atop the bone marrow stromal cell hierarchy, Sci. Rep. 7 (2017) 4928, https://doi.org/10.1038/s41598-017-05401-1.

[49] A. Hosoya, H. Nakamura, T. Ninomiya, K. Hoshi, K. Yoshiba, N. Yoshiba, M. Takahashi, T. Okabe, N. Sahara, H. Yamada, E. Kasahara, Hard tissue formation in subcutaneously transplanted rat dental pulp, J. Dent. Res. 86 (2007) 469–474, https://doi.org/10.1177/154405910708600515.

[50] A. Vijaykumar, S. Ghassem-Zadeh, I. Vidovic-Zdrilic, K. Komitas, I. Adameyko, J. Krivanek, Y. Fu, P. Maye, M. Mina, Generation and characterization of DSPP-Cerulean/DMP1-Cherry reporter mice, Genesis 57 (2019), e23324, https://doi.org/10.1002/dvg.23324.

[51] D.J. Hunter, C. Bardet, S. Mouraret, B. Liu, G. Singh, J. Sadoine, G. Dhamdhere, A. Smith, X.V. Tran, A. Joy, S. Rooker, S. Suzuki, A. Vuorinen, S. Miettinen, C. Chaussain, J.A. Helms, Wnt acts as a prosurvival signal to enhance dentin regeneration, J. Bone Miner. Res. 30 (2015) 1150–1159, https://doi.org/10.1002/jbmr.2444.

[52] T. Standal, R.W. Johnson, N.E. McGregor, I.J. Poulton, P.W. Ho, T.J. Martin, N. Sims, gp130 in late osteoblasts and osteocytes is required for PTH-induced osteoblast differentiation, J. Endocrinol. 223 (2014) 181–190, https://doi.org/10.1530/JOE-14-0424.

[53] N. Amizuka, M.Y. Kwan, D. Goltzman, H. Ozawa, J.H. White, Vitamin D3 differentially regulates parathyroid hormone/parathyroid hormone-related peptide receptor expression in bone and cartilage, J. Clin. Invest. 103 (1999) 373–381, https://doi.org/10.1172/JCI3265.

[54] T. Kobayashi, U.I. Chung, E. Schipani, M. Starbuck, G. Karsenty, T. Katagiri, D. L. Goad, B. Lanske, H.M. Kronenberg, PTHrP and Indian hedgehog control differentiation of growth plate chondrocytes at multiple steps, Development 129 (2002) 2977–2986.

[55] B. He, R.A. Deckelbaum, D. Miao, M.L. Lipman, M. Pollak, D. Goltzman, A. C. Karaplis, Tissue-specific targeting of the pthrp gene: the generation of mice with floxed alleles, Endocrinology 142 (2001) 2070–2077, https://doi.org/10.1210/endo.142.5.8146.

[56] Y. Qin, W. Chen, G. Jiang, L. Zhou, X. Yang, H. Li, X. He, H.L. Wang, Y.B. Zhou, S. Huang, S. Liu, Interfering MSN-NONO complex-activated CREB signaling serves as a therapeutic strategy for triple-negative breast cancer, Sci. Adv. 6 (2020), https://doi.org/10.1126/sciadv.aaw9960 eaaw9960.